Pergamon

Geochimica et Cosmochimica Acta, Vol. 63, No. 18, pp. 2785–2804, 1999

0016-7037/99 $20.00 + .00

PII S0016-7037(99)00158-1

Seafloor hydrothermal clay alteration at Jade in the back-arc Okinawa Trough: Mineralogy, geochemistry and isotope characteristics

KATSUMI MARUMO[1,*] and KÉIKO H. HATTORI[2]

[1]Mineral and Fuel Resources Department, Geological Survey of Japan, Higashi 1-1-3, Tsukuba, Ibaraki, 305, Japan
[2]Ottawa-Carleton Geoscience Centre, and Department of Earth Sciences, University of Ottawa, Ottawa, K1N 6N5, Canada

(*Received December* 17, 1996; *accepted in revised form April* 7, 1999)

Abstract—Seafloor hydrothermal activity at Jade has resulted in extensive alteration of the host epiclastic sediments and pumiceous tuffs, forming mica, kaolins (kaolinite and halloysite), Mg-rich chlorite, talc, montmorillonite, and a mixed-layer mineral of dioctahedral chlorite and montmorillonite (Chl/Mont). Clay mineral assemblages show a vertical variation, which reflects variable amounts of cold seawater incorporated into hot hydrothermal fluids in subsurface sediments and tuff. However, mixing alone cannot explain the occurrence of abundant kaolin minerals at Jade. The formation of kaolin minerals requires much more acidic fluid than expected from simple mixing of hydrothermal fluids and cold seawater. Low pH values are likely attained by oxidation of H_2S either dissolved in the hydrothermal fluid or released from the fluid during decompression. The fluid reaching the seafloor is discharged into cold seawater, which caused precipitation of sulfides close to vents and native sulfur and barite at the margins of the vent areas.

Halloysite, barite and anhydrite show Sr isotope compositions similar to marine Sr, indicating the derivation of marine Sr directly from seawater or by the dissolution of calcareous nannoplanktons. The isotopic compositions of kaolinite ($\delta^{18}O = +7.4‰$, $\delta D = -23‰$), Chl/Mont ($\delta^{18}O = +7.0‰$, $\delta D = -32‰$), and mica ($\delta^{18}O = +5.4$ to $+9.9‰$, $\delta D = -30$ to $-26‰$) suggest fluids of a heated seawater origin. The O isotopic data yielded formation temperatures of 170°C for kaolinite, 61 to 110°C for halloysite, and 145 to 238°C for mica.

Barite $\delta^{34}S$ values ($+21.0$ to $+22.5‰$) are very similar to the marine sulfate value, confirming that the barite formation took place due to mixing of Ba-bearing hydrothermal fluids and sulfate-rich seawater. Native sulfur shows a large variation in $\delta^{34}S$ in one hand specimen probably because of rapid disequilibrium precipitation of S during fluid exhalation on the seafloor. Sulfur in hydrothermal fluids is usually consumed to form metal sulfides. Therefore, abundant native sulfur at Jade suggests high H_2S/metals ratios of the hydrothermal fluids.

The alteration assemblages and isotopic data of hydrothermal minerals from Jade are very similar to those of Kuroko-type barite deposits of middle Miocene age, which formed from fluids of high S/metals ratios at less than 200°C.

At Jade, there is only one black smoker actively discharging high temperature (~320°C) fluid, but there are many fossil sulfide chimneys and mounds in the area. The mineralogy and high Au and Cu in these precipitates suggest highly metalliferous hydrothermal activity in the past. These activities likely resulted in discharge of hydrothermal plumes and fall-outs of sulfides and sulfates on the seafloor. These fall-outs were incorporated in sediments far from the vent areas. They are now recorded as high metal contents in sediments with no petrographic and mineralogical evidence of in-situ hydrothermal activity. Some are high as 8,100 ppm for Cu, 12,500 ppm for Zn, 1,000 ppm for As, 100 ppm for Ag and 21,000 ppm for Pb. Detrital grains of montmorillonite in such sediments are coated with Fe-oxyhydroxides during the suspension in seawater before settling on the seafloor. The depths of such metal anomalies in sediments suggest high levels of metalliferous hydrothermal activities from 1,800 to 300 ybp.

1. INTRODUCTION

In the subsurface of seafloor hydrothermal systems, ascending hot fluids change their compositions and temperatures by incorporating cold seawater. This leads to precipitation of hydrothermal minerals; such as sulfides, sulfates and clay minerals in subsurface sediments and tuffs. On the seafloor, an injection of hot fluids into seawater results in a rapid temperature drop and precipitation of minerals. The mineralogy and composition of sediments and hydrothermal minerals reflect the evolution of fluids through mixing with cold seawater beneath and on the seafloor.

Venting hydrothermal fluids occasionally produce plumes containing minute particles of sulfides and sulfates. Fall-out of these particles could be widely dispersed and incorporated into sediments. Metal anomalies in sediments may provide the evidence for past hydrothermal activity.

Many fossil seafloor hydrothermal deposits, known as stratabound massive sulfide deposits, were subject to deformation, diagenesis and metamorphism after their mineralization. The middle Miocene Kuroko-type sulfide deposits in Japan are considered to be the most well preserved fossil seafloor hydrothermal systems (Franklin et al., 1981), but their original features have already been modified during diagenesis and deformation (e.g., Ohmoto et al., 1983; Eldridge et al., 1983). The Jade deposit in the central Okinawa Trough (Fig. 1-1) is con-

*Author to whom correspondence should be addressed (marumo@gsj.go.jp).

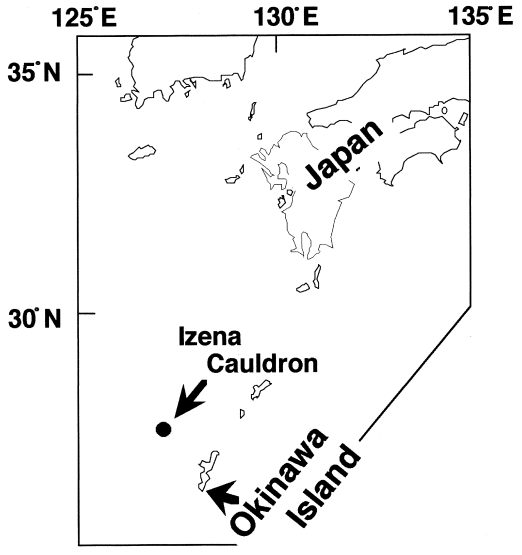

Fig. 1-1. Location of the Izena Cauldron.

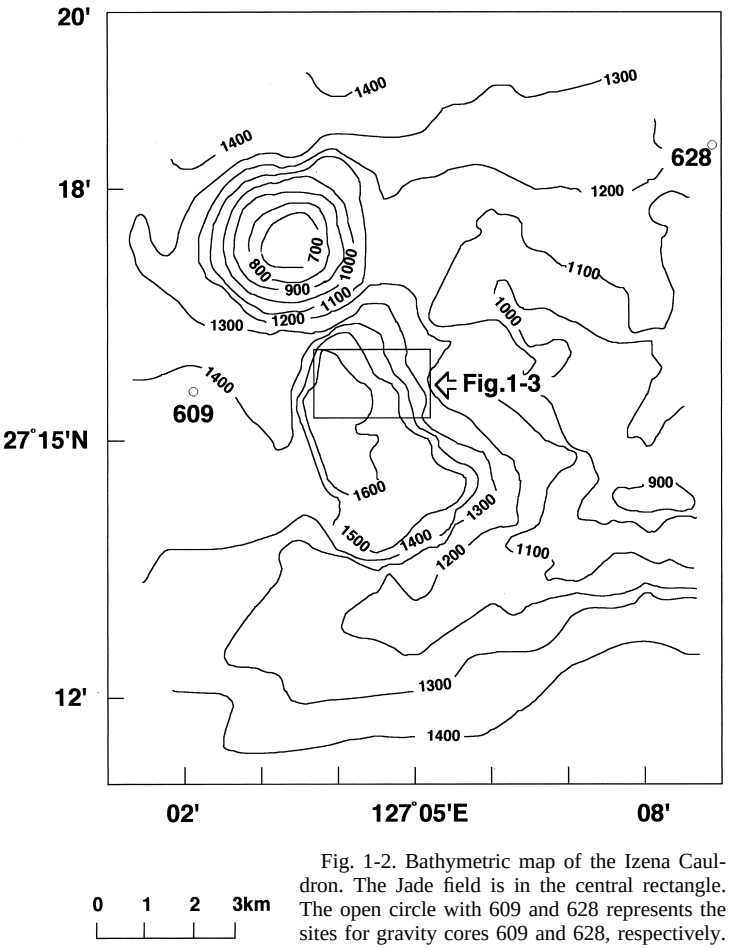

Fig. 1-2. Bathymetric map of the Izena Cauldron. The Jade field is in the central rectangle. The open circle with 609 and 628 represents the sites for gravity cores 609 and 628, respectively.

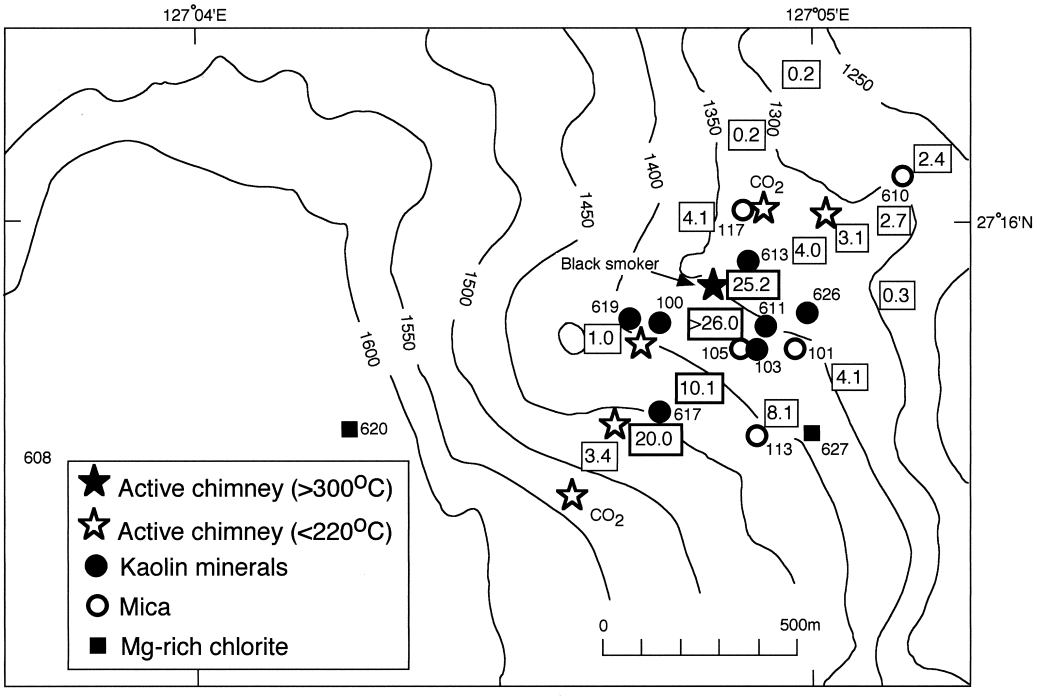

Fig. 1-3. Bathymetric map of the Jade field with the distribution of clay minerals. The sites for the gravity cores are numbered from 608 to 627 and those for the grab samplers from 100 to 117. Numbers in squares are heat flow values in kmW/m^2 (Kinoshita, 1990).

sidered to be a modern analogue of polymetallic Kuroko-type sulfide deposits (Halbach et al., 1989a; Sakai et al., 1990a, 1990b; Halbach et al., 1993). This paper describes mineralogical, geochemical and isotopic data of sediments and tuffs obtained from gravity corers and grab samplers in and around the Jade deposit. We discuss factors controlling the alteration and compare the data with those from two types of Kuroko-type deposits in Japan; the Kosaka polymetallic deposit (25 million tons ore with 2.2 wt% Cu, 4.5 wt% Zn, and 0.8 wt% Pb, Tanimura et al., 1983) and the Minamishiraoi barite deposit (0.2 million tons ore with over 90 wt% barite; Marumo, 1989a). The sulfide/barite wt% ratios are greater than 10 at Kosaka (Farrell and Holland, 1983) and less than 0.1 at Minamishiraoi (Marumo, 1989a).

2. GEOLOGY OF THE JADE DEPOSIT

The Okinawa Trough is a back-arc basin behind the Rhukyu island arc (Fig. 1-1) and it started rifting about 2 Ma (Lee et al., 1980; Letouzey and Kimura, 1986; Nagumo et al., 1986). The volcanic rocks in the trough are basalt, basaltic andesite, dacitic andesite, and rhyolite. High ^{3}He in He dissolved in the seawater [$(^3He/^4He)/(^3He/^4He)_{air} < 1.65$; Ishibashi et al., 1988] and high heat flow (up to 2,000 mW/m^2) suggest the presence of shallow magma chambers in the area (Yamano et al., 1989).

The Jade deposit is located along the NE slope of the tectonic depression named the Izena Cauldron (3 × 5 km) at water depths between 1,400 to 1,450 m (Figs. 1-2 and 1-3). The Cauldron is underlain by epiclastic sediments and pumiceous tuffs. Hydrothermal activity occurs along an ENE-striking fissure in the Cauldron, suggesting the fluid ascent through this fissure. The area along the fissure shows high heat flow (Fig. 1-3) and one black smoker is discovered in the highest heat flow area (over 10,000 mW/m^2; Kinoshita, 1990). The smoker discharges Mg^{2+}-free fluids of 320°C. There are chimneys discharging clear solutions of up to 220°C and they are accompanied by precipitates of Zn-Pb-rich sulfides, barite and anhydrite (Nakamura et al., 1990).

Fossil chimneys and sulfide mounds are abundant in the area and the sulfide samples from these mounds contain higher concentrations of Au (up to 4.8 ppm), Ag (up to 1,900 ppm), Pb (up to 9.3 wt%), Zn (up to 20.1 wt%), and Cu (up to 3.7 wt%), Sb (up to 1.4 wt%), As (up to 10.8 wt%), Hg (up to 1,670 ppm) and Tl (up to 1,440 ppm) than those from the precipitates at the black smoker (Nakamura et al., 1990). Crusts of native sulfur and barite on the seafloor occur in the areas with low heat flow (less than 3,000 mW/m^2; Kinoshita, 1990).

3. SAMPLING AND ANALYTICAL PROCEDURES

Epiclastic sediments and pumiceous tuffs were obtained using shipboard gravity corers (core penetration ranged from 1 to 5 m) and grab samplers during the transponder navigated R/V Hakurei-maru GH89-3 cruise in 1989. Samples are collected at 5 to 10 cm intervals in the cores. The locations of cores (sites 608 to 628) and grab samples (sites 100 to 117) are presented in Figs. 1-2 and 1-3.

The samples were air-dried and ground to <10 μm for major, minor, and trace element analysis, and bulk X-ray diffraction (XRD) analysis. The major and minor elements were determined using an X-ray fluorescence spectrometer (XRF) with a Rh tube at 4 to 50 kV and 0.35 mA. X-ray tube voltages were set at 4 kV for Al and Si; 15 kV for S, K, Ca, Ti, Mn and Fe; and at 50 kV for Sr, Y, Zr, Nb, and Ba. Other elements were determined using an inductively coupled plasma emission spectrometer for Na, Mg, P, Cu, Zn, Cd, and Pb, and atomic absorption spectrometer for As, Ag, Sb, and Hg after digestion of samples using HF-$HClO_4$-HNO_3.

The XRD analysis was performed on clay-size fractions of samples both on randomly oriented and oriented samples using a Cukα radiation source (140 mA and 60 kV), 1° divergence and scatter slits. The clay-size fractions were obtained by suspending samples in de-ionized water.

The ratios of Mg, Al, Si, and Fe for clay minerals were obtained from X-ray intensities of these elements using an analytical transmission electron microscope (ATEM) with an energy dispersive spectrometer at 100 kV accelerating voltage. To obtain K factors (Lorimer, 1987) of elements, the standards were prepared from finely ground (less than 2 μm) minerals (talc, Mg-rich chlorite, biotite, and nontronite) used as standards for electron microprobe analysis.

Iron coating on the surface of clay minerals was removed using hydroxylamine 25% hydrochloride acetic acid (HHAA) at pH 5.0 at 100°C for 6 hr (Tessier et al., 1979).

The clay samples were rinsed twice and cleaned in distilled water in an ultrasonic bath for 10 min for Sr-isotope analysis. Strontium on the surface and in the exchangeable sites was likely removed during the sample preparation which involved suspension of samples in distilled water for at least one week. Sr isotopic compositions were determined after HF-HNO_3 digestion followed by cation separation using Bio Rad AG 50W X8 (200–400 mesh). Strontium was eluted using 2.5 N HCl. Dissolution of barite was carried out by heating the mixture of barite and graphite at 1,000°C. Dissolved cations were separated by the procedure described above. Strontium in anhydrite was leached by 6 N HCl. All acids used for digestion and cation separation were double-distilled in Teflon. The Sr isotopic measurements were carried out using a Finnigan MAT261 and ratios were normalized to $^{86}Sr/^{88}Sr = 0.1194$. The 2 σ are all $<0.003\%$ of the reported values and the NBS 987 yielded 0.710247 ± 12 ($N = 14$) during this study.

The D/H ratios of clay minerals were measured on the H_2O extracted from the samples at 1,000°C, after removing absorbed and interlayer water in vacuum at 200°C (Savin and Epstein, 1970). The H_2O was reduced to H_2 on U metal at 800°C. For the $^{18}O/^{16}O$ analysis, O was extracted from the clay minerals using the BrF_5 method of Clayton and Mayeda (1963) after pre-heating the samples under vacuum at 200°C for 20 hrs. These H and O isotope data are reported in the conventional δ-notation relative to SMOW.

For S isotope analysis, a mixture of a sample and Cu_2O was heated to 1,050°C to produce SO_2 for the mass spectrometric analysis. The yields of gases were monitored by measuring the pressures of SO_2, CO_2 and H_2.

4. RESULTS

4.1. Geochemistry and Mineralogy of Epiclastic Sediments outside the Izena Cauldron

Vertical compositional variations of sediments are shown at two sites: site 628, 8 km NE from the Izena Cauldron (Fig. 2-1), and site 609, 2.5 km W (Fig. 2-2) from the edge of the Cauldron. The sites show normal heat flow values (less than 160 mW/m^2; Kinoshita, 1990) for the Okinawa Trough and the sediments consist of quartz, feldspars, mica, Fe-Mg-chlorite, and Ca-montmorillonite all of detrital origin. High CaO (up to 36 wt.%) and Sr (up to 1,260 ppm) in the samples of P609-5-5-75, P609-4-5-55, P628-4-4-10, and P628-4-4-70 (Table 1) reflect abundant calcareous nannoplanktons (*emiliania huxleyi* and *florisphaera profunda*; Tanaka, 1990). There is no evidence for hydrothermal alteration, but the sediment samples contain high Cu (up to 240 ppm), Zn (up to 628 ppm), Cd (up to 6 ppm), Ba (up to 1,025 ppm), Hg (up to 9 ppm) and Pb (up to 1,145 ppm) from the surface to a depth of 100 cm (Fig. 2-2). The highest Zn (628 ppm) and Hg (9 ppm) were recorded at a depth of 75 cm (sample P609-4-5-35, Table 1); whereas the highest As concentration (25 ppm) was in the surface sample

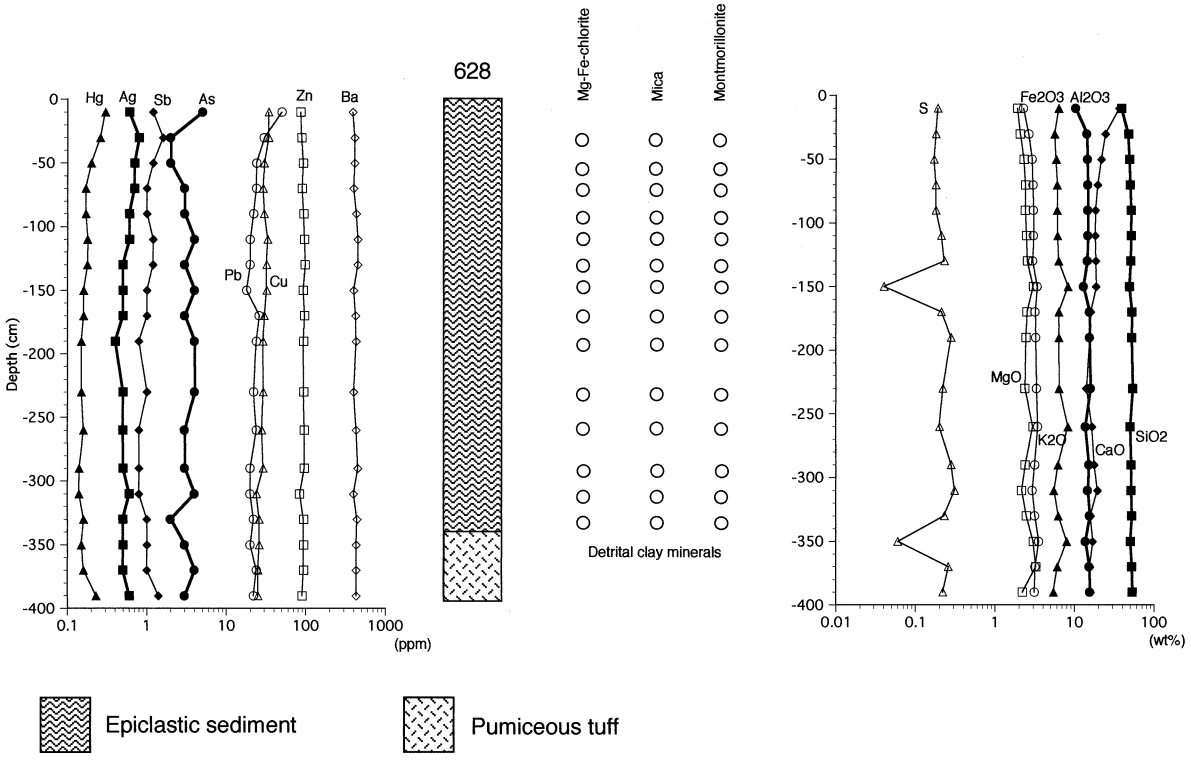

Fig. 2-1. Vertical section of the gravity core at site 628, 8 km NE of the Izena Cauldron. The location of the core is shown in Fig. 1-2. The wavy pattern and the diagonally cross hatched area in the section represent epiclastic sediments and tuffs, respectively.

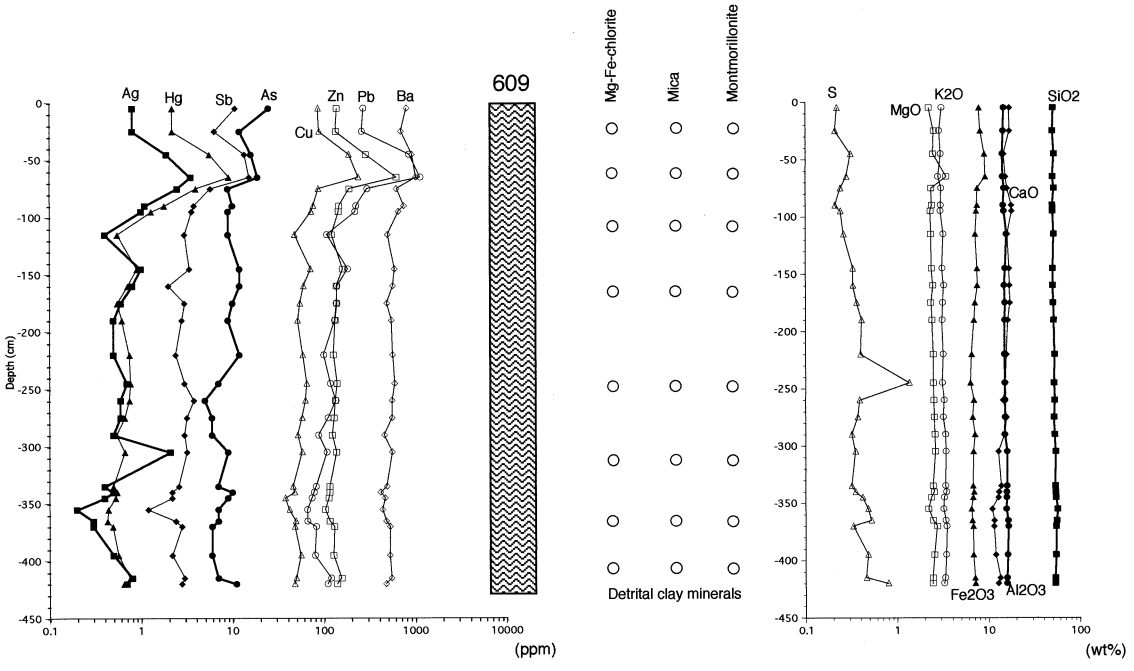

Fig. 2-2. Vertical section of the gravity core at site 609, 2.5 km W of the Izena Cauldron. The site of the core is shown in Fig. 1-2. The wavy patterned area represents epiclastic sediments.

(P609-5-5-75, Table 1). The lack of alteration suggests that the metal enrichment is not caused by in-situ hydrothermal activity. Therefore, the metal anomalies are attributed to fall-out from hydrothermal plumes. Sulfides and sulfates in plumes could be dispersed and incorporated into sediments, far from the vent site.

Detrital montmorillonite in these samples shows high atomic ratios of Fe/(Mg+Al+Fe) ranging from 0.38 to 0.60, but the

Table 1. Mineral assemblages and chemical compositions of epiclastic sediments (H_2O and CO_2 free basis).

Sample no.	P609-5-5-75	P609-4-5-35	P609-4-5-55	P611-2-3-40	P611-2-3-65	P611-2-3-90	P617-2-2-95	P626-1-5-75	P627-2-2-20	P627-2-2-76	P628-4-4-10	P628-4-4-70
Depth (cm)	15	75	95	120	145	170	5	470	20	76	10	70
Mineralogy	Mg-Fe-chl Mica, Mont Pl, Qtz, Cal	Mg-Fe-chl Mica, Mont Pl, Qtz, Cal	Mg-Fe-chl Mica, Mont Pl, Qtz, Cal	Halloysite* Qtz, Py* Marc*, Sph*	Talc*, Mg-chl* Qtz, Py, Marc* Sph*, Cp* Gl*, Brt*	Talc*, Mg-chl* Qtz, Py, Marc* Sph*, Cp* Brt*	Mg-Fe-chl Mica, Mont Pl, Qtz Sph*, Brt*	Mont* Qtz Py* zztabftr;*	Mg-Fe-chl Mica, Mont Pl, Qtz, Cal	Mg-Fe-chl Mica, Mg-chl* Pl, Qtz, Py* Marc*, Sph* Gl*, Brt*	Mg-Fe-chl Mica, Mont Pl, Qtz Cal	Mg-Fe-chl Mica, Mont Pl, Qtz, Cal
	Major elements (wt%)											
SiO_2	50.94	50.50	50.95	51.76	58.86	61.92	59.12	57.57	56.10	57.58	38.80	50.26
TiO_2	0.78	0.74	0.81	0.55	0.87	0.69	0.84	0.61	0.86	0.86	0.73	0.77
Al_2O_3	14.64	14.34	15.01	33.30	10.57	12.67	16.93	26.94	16.59	21.36	10.31	14.71
Fe_2O_3 (total)	7.88	9.31	7.44	6.55	2.65	4.45	8.10	6.09	7.55	6.12	6.30	6.05
MnO	0.11	0.10	0.13	0.07	0.03	0.02	0.11	0.06	0.12	0.04	0.08	0.07
CaO	16.96	15.42	16.99	0.18	0.38	0.24	0.41	0.27	9.64	0.80	36.38	19.53
MgO	2.23	3.47	2.40	0.51	14.14	11.05	1.88	1.06	2.51	4.93	1.91	2.41
Na_2O	2.99	2.61	2.80	2.78	2.87	3.54	2.78	2.91	2.84	2.22	2.88	2.87
K_2O	3.09	2.83	2.95	0.90	0.97	1.63	2.74	1.90	3.21	2.27	2.29	2.99
P_2O_5	0.18	0.18	0.17	0.16	0.00	0.04	0.06	0.07	0.10	0.07	0.14	0.12
S (total)	0.22	0.28	0.32	3.44	4.17	3.15	6.10	2.49	0.20	3.20	0.19	0.18
	Minor and trace elements (ppm)											
V	110	189	111	27	102	108	133	100	130	115	64	82
Cr	72	141	88	25	55	139	148	2	105	91	62	75
Cu	87	240	82	189	8,490	914	285	576	169	576	34	29
Zn	140	628	160	1,125	11,200	8,960	1,100	332	466	2,340	86	90
As	25	19	9	140	350	145	180	140	24	740	5	23
Rb	139	125	131	13	21	50	98	125	112	60	111	137
Sr	639	620	687	61	124	328	273	106	387	254	1,264	884
Y	20	<5	25	25	<5	<5	<5	<5	12	<5	29	19
Zr	155	157	165	265	99	75	113	229	119	125	165	152
Nb	14	11	15	19	<5	7	12	9	7	9	10	13
Mo	<1	<1	<1	207	93	162	111	7	23	34	<1	<1
Ag	1	4	1	2	>100	38	8	1	3	66	1	3
Cd	1	7	1	3	112	26	7	1	6	96	1	1
Sb	11	15	5	11	550	385	51	14	12	110	1	1
Ba	743	1,025	642	197	20,000	1,331	9,015	10	2,921	3,398	517	255
Hg	2	9	1	3	43	30	18	8	4	26	<1	<1
Pb	274	1,145	268	508	9,030	34	600	160	196	2,500	50	24

* Hydrothermal minerals.

Mg-Fe-chl = Mg-Fe-chlorite, Mont = montmorillonite, Mg-chl = Mg-rich chlorite, Pl = Na, K, Ca feldspars, Qtz = quartz, Cal = calcite, Py = pyrite, Marc = marcasite, Sph = sphalerite, Cp = calcopyrite, Gl = galena, Brt = barite.

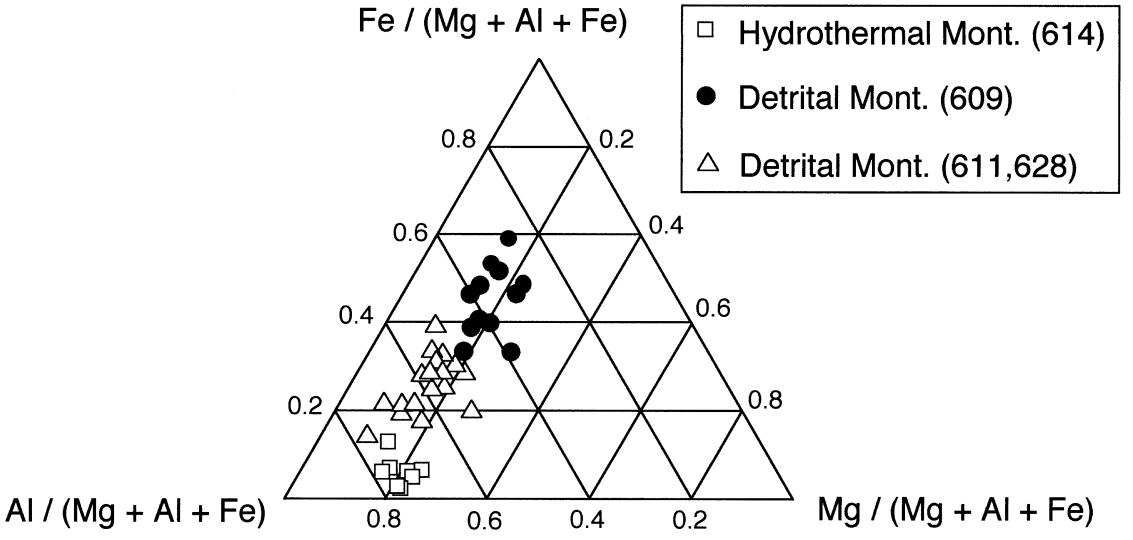

Fig. 3-1. Mg, Al, and Fe atomic ratios of montmorillonite. Open squares represent hydrothermal montmorillonite from site 614. Solid circles are those for detrital montmorillonite from site 609. Open triangles are ratios for detrital montmorillonite from sites 611 and 628.

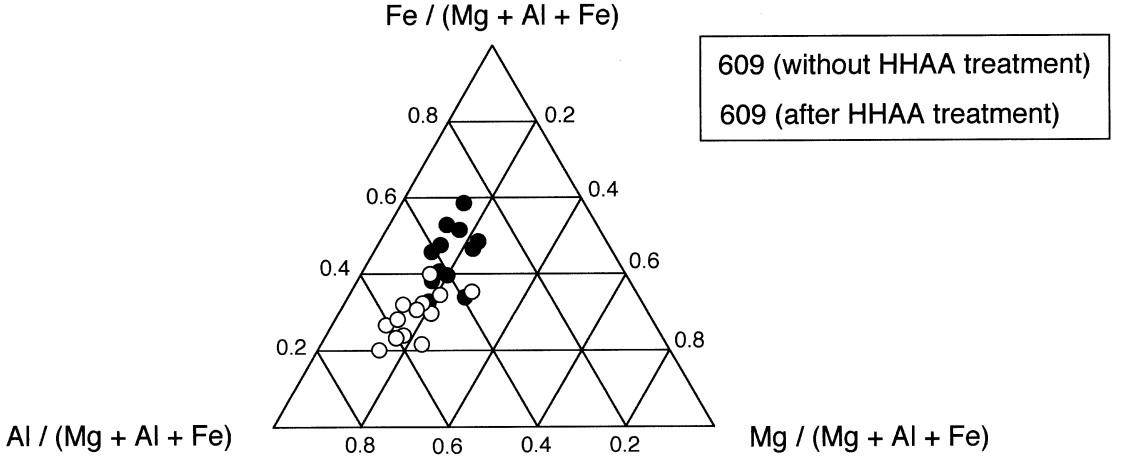

Fig. 3-2. Mg, Al, and Fe atomic ratios of the detrital montmorillonite from site 609. Solid circles represent the ratios before the treatment using hydroxylamine 25% hydrochloride-acetic acid (HHAA). Open squares are those after the treatment. Note that the compositions after the treatment are similar to those of detrital montmorillonite shown in Fig. 3-1.

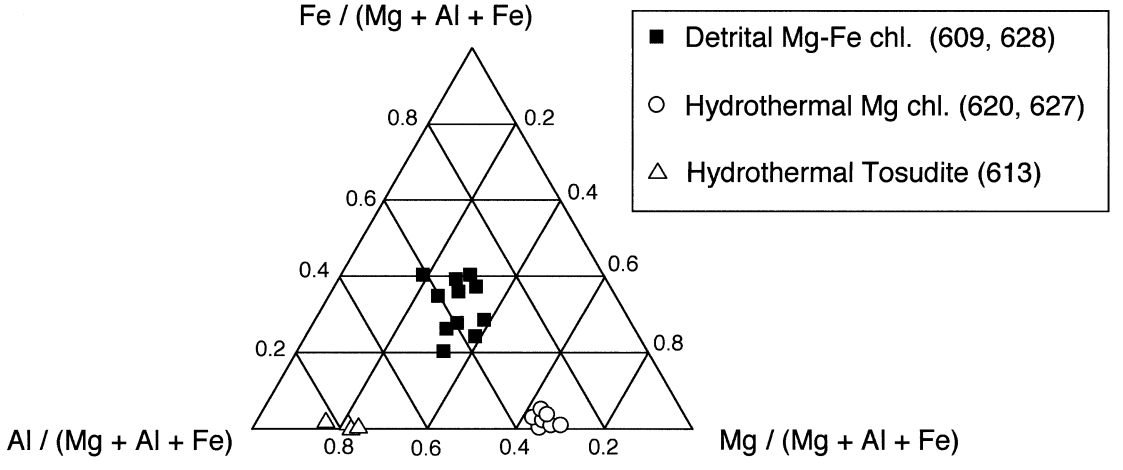

Fig. 3-3. Mg, Al, and Fe atomic ratios of chlorite. Solid squares are ratios for detrital Mg-Fe-chlorite from sites 609 and 628. Open circles are ratios for hydrothermal chlorite from sites 620 and 627. Open triangles are those for tosudite from site 613.

ratios decrease to 0.20 to 0.40 after HHAA treatment. The latter values are similar to those from the site 628 (Figs. 3-1 and 3-2), suggesting that the montmorillonite is of detrital origin and that the grains yielded apparently high Fe contents due to coating of Fe oxyhydroxide.

It is not surprising to find Fe-coated montmorillonite because the surface of clay minerals has net negative charges in neutral to alkaline water (Sverjensky and Sahai, 1996) and attracts high valance cations, such as Fe^{3+}. Montmorillonite grains with Fe coating have been reported at the Galapagos hydrothermal mound field (McMurtry et al., 1983) and the EPR and Bauer Basin sediments (McMurtry and Yeh, 1981).

4.2. Geochemistry and Mineralogy of Epiclastic Sediments in the Izena Cauldron

Table 1 shows the chemical compositions of the epiclastic sediments around the active vent areas (sites 611, 617, 626, 627; Fig. 1-3). Calcium-rich samples contain calcareous nannoplanktons (sample P627-2-2-20, Table 1), but many samples show CaO contents lower than 1.03 wt% and they do not contain nannoplanktons, due to their dissolution by acidic fluid.

Chemical compositions and mineral assemblages of these epiclastic sediments vary in one gravity core. For example at site 627, CaO contents vary from 9.64 wt% at a depth of 20 cm (sample P627-2-2-20; Table 1) to less than 1 wt% at 76 cm depth (sample P627-2-2-76; Table 1). The latter sample is characterized by high concentrations of MgO (4.93 wt%), Cu (576 ppm), Zn (2,340 ppm), As (740 ppm), Ag (66 ppm), and Pb (2,500 ppm). The high concentration of MgO is reflected by the occurrence of hydrothermal Mg chlorite, which, using ATEM, is easily distinguished from detrital Fe-Mg chlorite (Fig. 3-3).

The epiclastic sediments at site 611 show a chemical and mineralogical variation within a meter (Fig. 4-1). They still contain detrital minerals of feldspars, mica, Mg-Fe-chlorite, and Ca-montmorillonite, but they are partly or entirely altered. Halloysite occurs at a depth of 120 cm and in the interval between 230 and 275 cm depths, and talc and Mg-rich chlorite occur at 135 to 170 cm depths. Talc-bearing sediments contain high concentrations of MgO (up to 14.14 wt%), Cu (up to 1.1 wt%), Zn (up to 8.5 wt%), As (up to 2,000 ppm), Ag (up to 100 ppm), Ba (up to 2.0 wt%), Hg (up to 43 ppm), and Pb (up to 9,000 ppm), whereas halloysite-bearing sediments contain low concentrations of Cu (less than 250 ppm), Zn (less than 1,445 ppm), As (less than 140 ppm), Ag (less than 2 ppm), Ba (less than 520 ppm), Hg (less than 3 ppm), and Pb (less than 1,815 ppm).

4.3. Geochemistry and Mineralogy of Pumiceous Tuffs

Site 620 shows a high heat flow value (871 mW/m^2), which is much higher than background values but lower than those near the active vents (over 1,000 mW/m^2; Fig. 1-3; Kinoshita, 1990). Both sediments and tuffs at the site are intensely altered to show low concentrations of CaO, (less than 1.3 wt%, Table 2). The tuffs contain high concentrations of MgO (up to 5.83 wt%), Zn (up to 8,100 ppm), Ba (up to 1,852 ppm), Pb (up to 1,580 ppm) with abundant Mg-rich chlorite of hydrothermal origin (Fig. 3-3).

Pumiceous tuffs close to the active vents (sites 613, 614, 619 and 626) are all intensely altered. The tuffs at the sites 613 and 626 contain kaolinite and halloysite, which is reflected by high Al/Si molar ratios, greater than 0.45, of the tuffs. These tuffs from the site 613 additionally contain K-montmorillonite, Chl/Mont, and mica of all hydrothermal origin.

Bulk samples from the sites 614 (sample P614-2-3-55) and 619 (samples P619-1-2-50, P619-1-2-95, and P619-1-2-Shoe top) show low Al/Si molar ratios (less than 0.38) similar to those of unaltered tuffs, but they contain abundant alteration minerals, such as K-montmorillonite. Hydrothermal montmorillonite is characterized by low Fe (Fig. 3-1). Furthermore, the tuff at the site 614 contains high concentrations of As, Sb and Hg (Table 2) and the tuffs at the site 619 contain hydrothermal mica, kaolinite, halloysite, and dolomite.

The gravity core at the site 613 shows a vertical zoning of alteration mineral assemblages: kaolinite and mica at depths shallower than 45 cm, Chl/Mont and kaolinite at depths from 45 to 70 cm and from 135 to 145 cm, halloysite at depths from 80 to 155 cm, and kaolinite and montmorillonite at a depth of 175 cm (Fig. 4-3). The kaolin-bearing pumiceous tuffs show higher concentrations of Al_2O_3, (over 35 wt%), and lower concentrations of K_2O (less than 0.63 wt%), CaO (less than 0.21 wt%), Ba (less than 111 ppm). The concentrations of Y (less than 254 ppm) and Zr (less than 459 ppm) are also high. The concentrations of Zn (up to 6,000 ppm), Sb (up to 55 ppm), Hg (up to 100 ppm), and Pb (up to 2,000 ppm) are high only close to the surface, shallower than 20 cm (Fig. 4-3).

Kaolinite from the site 613 (sample 613-2-2-60) is triclinic with split X-ray reflections of $(11\bar{1})$ and $(1\bar{1}\bar{1})$ (Fig. 5). Such a high structural integrity is observed only in hydrothermal kaolinite and is not observed in sedimentary kaolinite (Nagasawa, 1978). Halloysite (sample 613-1-2-50) is tabular (<0.05 μm width and <1 μm length) under TEM observation and has a disordered structure characterized by two-dimension (hk) bands and 7 Å basal spacing in the XRD diagram (Fig. 5). The XRD pattern of Chl/Mont (sample P613-2-2-90) is identical to that of a regularly interstratified dioctahedral chlorite and montmorillonite with a sharp reflection at about 30 Å and a (060) peak at about 1.499 Å (Fig. 5). The ATEM analysis (Fig. 3-3) shows the Chl/Mont to be an Al-rich and Mg-poor member (tosudite).

Mica is the predominant clay in the pumiceous tuffs at the site 113 (Fig. 1-3). The XRD pattern of the sample RS113 suggests that it is a mixture of 1M and $2M_1$ types or $2M_2$ type (Fig. 5).

4.4. Strontium Isotope Compositions of Clay Minerals and Sulfates

The Sr isotopic compositions are presented in Table 3 and Fig. 6. The $^{87}Sr/^{86}Sr$ ratios of halloysite (0.70902) from the site 613, barite crusts (0.70905 to 0.70915) from the sites 611, 110 and 113 and anhydrite (0.70910) from the black smoker vent are very similar to that of the present-day seawater value (0.70910; Koepnick et al., 1985), indicating marine Sr as the major source. The values are also similar to that for Sr dissolved in the black smoker vent fluids (0.7089; Chiba et al., 1992). Marine Sr is incorporated into hydrothermal fluids either

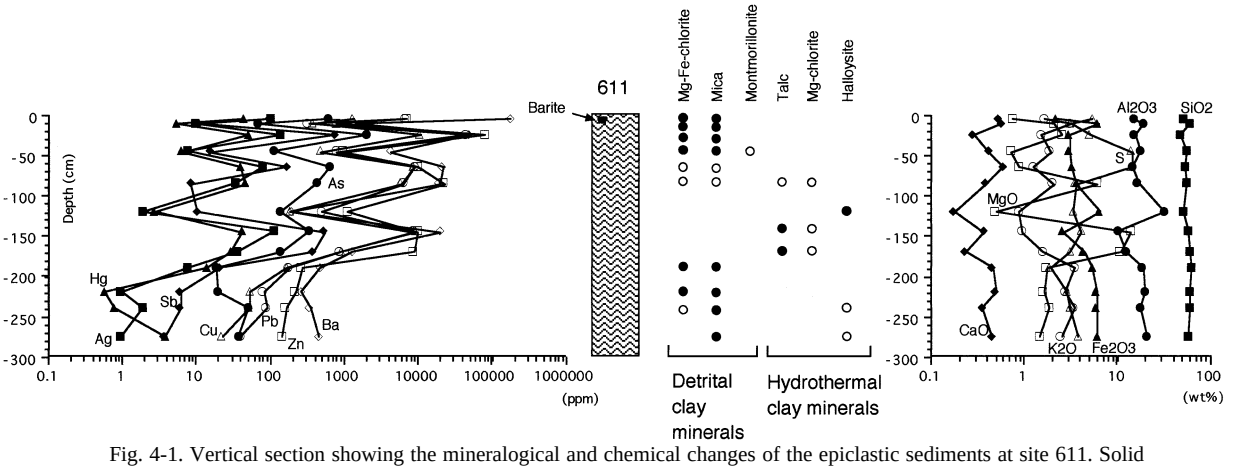

Fig. 4-1. Vertical section showing the mineralogical and chemical changes of the epiclastic sediments at site 611. Solid and open circles in the occurrences of clays denote major and minor occurrences, respectively.

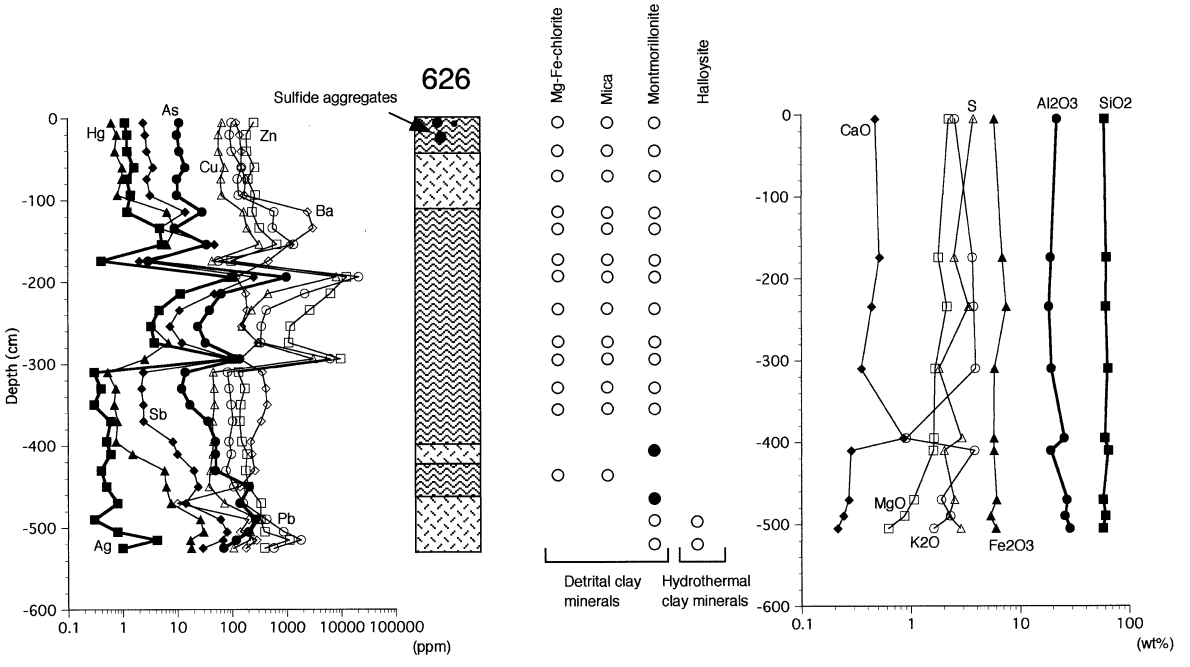

Fig. 4-2. Vertical mineralogical and compositional changes of the gravity core at site 626. The wavy pattern represents epiclastic sediments, the diagonally cross hatched area are tuffs. The solid circles near the surface show the occurrences of sulfide aggregates. The solid and open circles in the clay minerals assemblage denote major and minor occurrences, respectively.

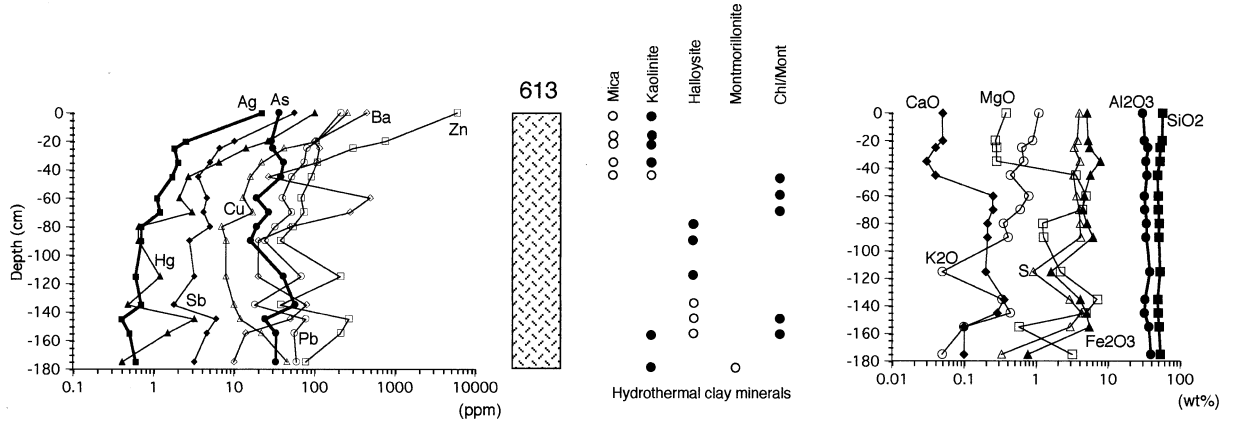

Fig. 4-3. Vertical section of the gravity core at site 613, showing the mineralogical and chemical changes of pumiceous tuffs (diagonally cross hatched area). Solid and open circles on the table denote major and minor occurrences, respectively.

Table 2. Mineral assemblages and chemical compositions of pumiceous tuff (H_2O and CO_2 free basis).

Sample no.	P608-1-3-5	P613-2-2-60	P613-2-2-90	P613-1-2-20	P613-1-2-50	P613-1-2-90	P614-2-3-55	P619-1-2-50	P619-1-2-95	P619-Shoe-T	P620-Shoe	P626-Shoe
Depth (cm)	205	25	55	85	115	155	150	70	115	140	120	510
Mineralogy	Mg-Fe-chl Mica, Mont Pl, Qtz, Cal	Kaolinite* Mica*, Qtz Py*, Marc*	Tosudite* Qtz, Py*	Halloysite* Py*, Marc*	Halloysite*	Kaolinite* Halloysite* Py*, Marc*	Mont* Py*, Brt*	Kaolinite* Mica*, Qtz Dolomite*	Kaolinite* Mica*, Qtz Dolomite*	Kaolinite* Mica*, Qtz Gl*, Dolomite*	Mg-chl* Mica, Qtz Sph*, Gl* Brt*	Halloysite* Qtz
	Major elements (wt%)											
SiO_2	51.94	52.57	49.38	50.46	53.07	50.88	60.91	65.14	64.77	65.72	63.30	60.59
TiO_2	0.82	0.62	0.68	0.70	0.81	0.74	1.10	0.82	0.81	0.82	0.66	0.72
Al_2O_3	14.77	35.88	32.32	33.71	38.27	36.99	19.70	20.07	20.64	21.33	16.96	25.95
Fe_2O_3 (total)	9.07	5.43	4.65	6.10	1.61	5.51	6.87	3.09	2.92	3.39	3.91	4.86
MnO	0.10	0.03	0.04	0.03	0.01	0.03	0.05	0.10	0.07	0.07	0.11	0.04
CaO	13.74	0.04	0.25	0.21	0.20	0.10	0.47	2.78	2.83	0.93	1.30	0.21
MgO	2.59	0.28	4.95	1.27	2.19	0.58	2.02	2.63	1.88	2.04	5.83	0.89
Na_2O	3.42	1.15	3.25	2.79	2.97	2.00	1.82	0.61	0.63	0.66	2.47	2.25
K_2O	3.11	0.63	0.79	0.41	0.05	0.10	1.45	3.60	4.46	3.56	2.83	2.17
P_2O_5	0.10	0.02	0.04	0.04	0.03	0.03	trace	0.13	0.11	0.14	0.10	0.04
S (total)	0.30	3.34	3.63	4.14	0.91	2.97	4.29	1.08	0.85	1.22	1.41	2.27
	Minor and trace elements (ppm)											
V	133	31	30	36	20	21	15	65	69	81	59	53
Cr	80	60	47	20	18	22	66	100	117	95	60	36
Cu	132	42	13	8	8	22	7	15	495	183	341	304
Zn	222	302	68	38	210	212	188	164	522	718	8,100	330
As	19	30	19	16	41	33	3,200	16	50	29	150	270
Rb	140	17	19	8	<5	5	39	111	138	111	72	82
Sr	587	161	306	78	189	795	1,470	39	28	59	100	65
Y	15	20	24	32	254	46	29	20	19	21	6	<5
Zr	153	421	340	351	459	441	167	170	133	169	132	238
Nb	12	14	13	18	14	17	9	14	13	13	6	8
Mo	<1	95	93	35	34	48	55	<1	<1	<1	12	31
Ag	3	2	1	1	1	1	1	0	1	1	6	0
Cd	1	3	1	<1	1	<1	<1	2	3	40	45	1
Sb	11	7	5	3	3	5	53	1	1	1	30	61
Ba	1,281	111	494	20	21	13	10,680	300	329	876	1,852	333
Hg	2	14	1	1	1	2	>100	<	<	<	3	26
Pb	450	80	40	24	68	56	<2	68	166	1,160	1,580	430

* Hydrothermal minerals.

Mg-Fe-chl = Mg-Fe-chlorite, Mont = montmorillonite, Mg-chl = Mg-rich chlorite, Pl = Na, K, Ca feldspars, Qtz = quartz, Cal = calcite, Py = pyrite, Marc = marcasite, Sph = sphalerite, Cp = calcopyrite, Gl = galena, Brt = barite.

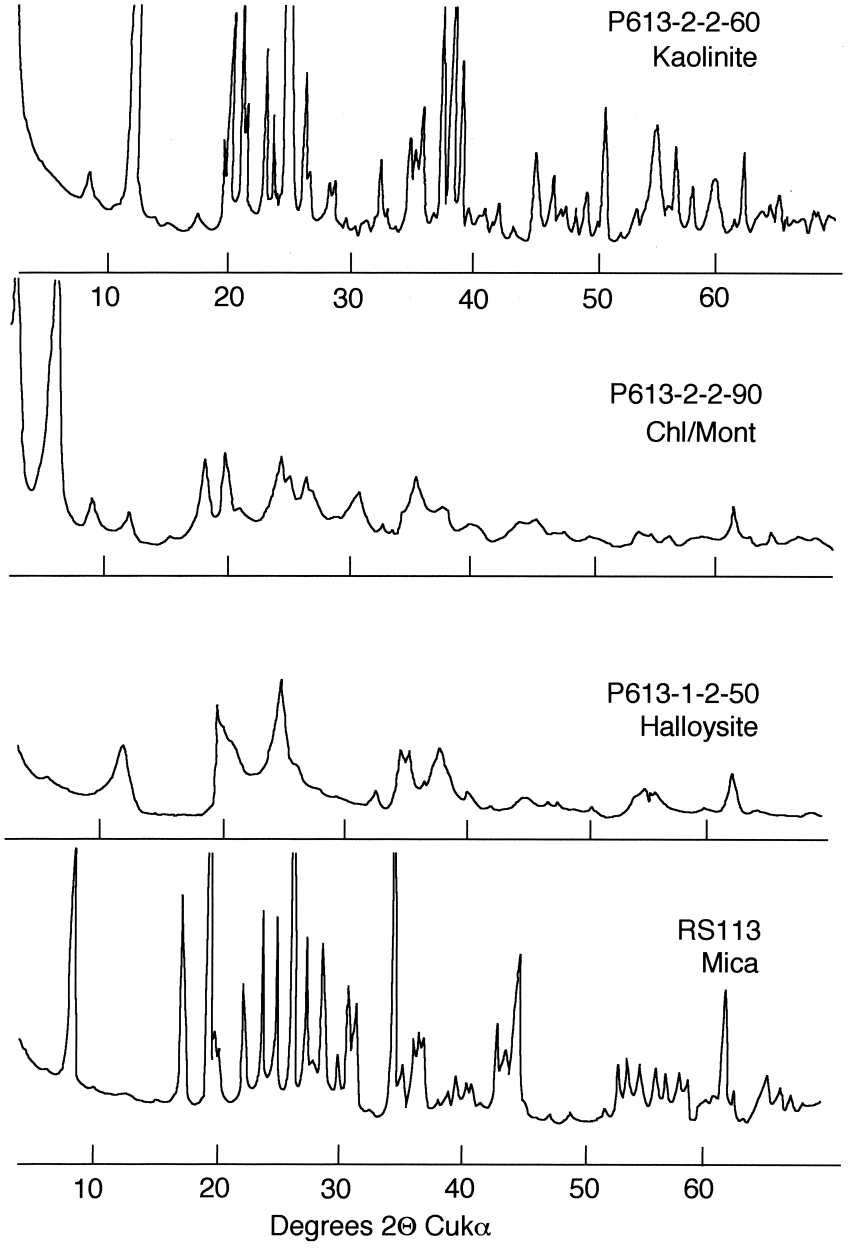

Fig. 5. Powder X-ray diffraction patterns of kaolinite, dioctahedral mixed-layer mineral of chlorite and montmorillonite (Chl/Mont, tosudite), halloysite, and mica.

directly through seawater or by the dissolution of calcareous nannoplanktons.

The $^{87}Sr/^{86}Sr$ of halloysite (P611-2-3-40) in an epiclastic sediment at the site 611 is 0.71085, which is higher than the seawater value. It is likely that Sr was probably derived from detrital minerals.

4.5. Hydrogen and Oxygen Isotope Compositions of Clay Minerals

The isotopic compositions of mica from the sites 105 and 113, kaolinite and Chl/Mont and halloysite from the sites 613 and 626 are presented in Figs. 7, 8, and 9 and Table 3. Formation temperatures of clay minerals were calculated using their $\delta^{18}O$ values, assuming that the parent fluids have the seawater value of 0‰. The calculation yielded 170°C for the formation temperature of kaolinite using the isotopic fractionation factor (α) between kaolinite and water expressed by $1000 \ln \alpha = 2.76 * 10^6/T^2 - 6.75$ (Sheppard and Gilg, 1996). The equation was derived from both experimental (Kulla and Anderson, 1978) and natural data (Lawrence and Taylor, 1972). The δD value of the fluid for the kaolinite is estimated using the equation, $1000 \ln \alpha = -2.05 * 10^6/T^2 - 11.13$, by Sheppard and Gilg (1996), which was derived from a combination of experimental (Kulla, 1979) and empirical calibration of natural

Table 3. Isotopic data of clay, sulfide, and sulfate minerals.

Sample no.	Location	Analyzed phases	δD (‰)	$\delta^{18}O$ (‰)
P613-2-2-60	613 core 25 cm depth	Kaolinite>>>Mica	−23	+7.4
P613-2-2-90	613 core 55 cm depth	Chl/Mont	−32	+7.0
P613-1-2-50	613 core 115 cm depth	Halloysite>>>Kaolinite	−53	+12.0
P613-1-2-90	613 core 155 cm depth	Halloysite>>>Kaolinite	−24	
P626-Shoe	626 core 510 cm depth	Halloysite	−34	+18.0
RS105	Surface sample	Mica	−26	+9.9
RS113	Surface sample	Mica	−30	+5.4
			$\delta^{34}S$ (‰)	
P613-2-2-60	613 core 25 cm depth	Pyrite>Marcasite	−14.5	
P613-2-2-70	613 core 35 cm depth	Pyrite>Marcasite	−18.2	
P613-1-2-20	613 core 85 cm depth	Marcasite>Pyrite	−14.4	
P613-1-2-70	613 core 135 cm depth	Marcasite>Pyrite	−19.3	
P617-1-2-5	617 core 10 cm depth	Marcasite>Pyrite	−18.1	
P617-1-2-25	617 core 30 cm depth	Marcasite>Pyrite	−4.7	
P617-1-2-55	617 core 60 cm depth	Marcasite>Pyrite	−7.9	
P617-1-2-75	617 core 80 cm depth	Marcasite>Pyrite	+0.7	
P617-1-2-85	617 core 90 cm depth	Marcasite>Pyrite	−22.0	
P617-Shoe	617 core 120 cm depth	Pyrite>Marcasite	−4.2	
P626-2-5-30	626 core 330 cm depth	Marcasite>Pyrite	−14.5	
P626-Shoe	626 core 510 cm depth	Marcasite>Pyrite	−32.7	
RS103	Surface sample	Marcasite>Pyrite	−15.4	
RS118	Surface sample	Marcasite>Pyrite	−38.5	
D412-4-1	Black smoker chimney	Sulfide aggregates*	+5.7	
RS101	Surface sample	Sulfide aggregates**	+3.2	
P626-5-5-15	626 core 15 cm depth	Sulfide aggregates**	+4.5	
P616-Shoe	Surface sample	Sulfide aggregates**	+6.1	
P626-3-5-5	626 core 205 cm depth	Barite	+22.5	
P626-Shoe	626 core 510 cm depth	Barite	+21.0	
RS109-A	Surface sample	Native sulfur	+6.6	
RS109-B	Surface sample	Native sulfur	+11.2	
RS109-C	Surface sample	Native sulfur	+10.2	
			Sr (ppm)	$^{87}Sr/^{86}Sr$
P611-2-3-40	611 core 120 cm depth	Halloysite	29	0.71085
P613-1-2-50	613 core 115 cm depth	Halloysite>>Kaolinite	75	0.70902
P611-3-3-5	611 core 5 cm depth	Barite		0.70915
RS110	Surface sample	Barite		0.70905
RS113	Surface sample	Barite		0.70952
D412-2	Surface sample from a black smoker	Anhydrite		0.70910

* Admixture of chalocopyrite-pyrite-sphalerite.
** Admixture of pyrite and marcasite.

samples (Lawrence and Taylor, 1972; Marumo et al., 1980). The calculated value is −1‰, which is similar to that of seawater. The results endorse the assumption of $\delta^{18}O = 0‰$ used for the calculation of isotopic temperatures.

The $\delta^{18}O$ and δD values of halloysite are +12.0‰ and −53‰ for the sample P613-1-2-50 and +18‰ and −34‰ for the sample P626-Shoe, respectively. The isotopic fractionation factors for halloysite are not well defined, but they can be approximated by the α values for kaolinite (Sheppard and Gilg, 1996) because of structural and chemical similarities of the two phases. The $\delta^{18}O$ yielded the formation temperatures for the halloysite in P613-1-2-50 and P626-Shoe at 110°C and 61°C, respectively. The δD values of the fluids are estimated to be −28‰ (P613-1-2-50) and −4‰ (P626-Shoe). The former value is significantly low and this low value is likely due to hydrogen isotopic exchange between interlayer water and hydroxyl ion. It has been documented in Quaternary soils (Lawrence and Taylor, 1971; Sheppard and Gilg, 1996) that hydroxyl H of halloysite can easily exchange with H in interlayer water even during the clay separation in laboratories because of immediate contact between the two H.

The $\delta^{18}O$ value (+5.4‰) of mica (sample RS113) is similar to those of micas from the Kosaka Kuroko-type deposit (+4.0 to +5.4‰; Hattori and Muehlenbachs, 1980), but another mica sample (RS105) shows a high value (+9.9‰), similar to those of Mica/Mont from the Minamishiraoi deposit (+7.5 to +9.2‰; Marumo et al., 1995). Both micas show higher δD (−30‰ for RS113, −26‰ for RS105) than Kosaka micas (−44 to −36‰; Hattori and Muehlenbachs, 1980) and similar δD to Mica/Mont with over 80% mica components from the Minamishiraoi deposit (−32 to −23‰; Marumo et al., 1995).

The formation temperatures of the Jade micas are calculated to be 238°C (RS113) and 145°C (RS105), using the isotopic fractionation factors between mica and water expressed by $1000 \ln \alpha = 2.39 * 10^6/T^2 - 3.76$ (Sheppard and Gilg, 1996). The equation was derived from a combination of experimental

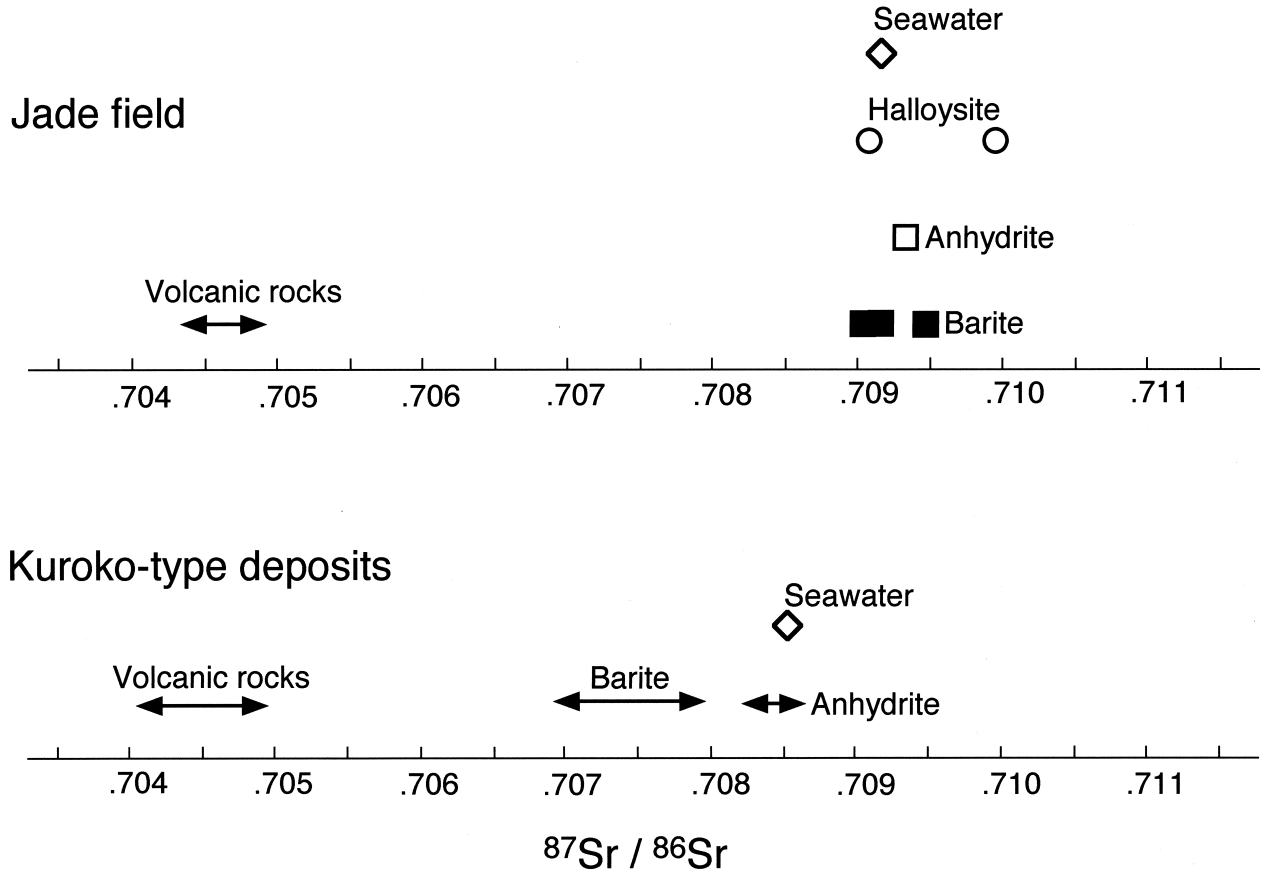

Fig. 6. Strontium isotopic compositions of halloysite, anhydrite and barite from the Jade field. The data are compared to those for the present and Miocene seawater (Koepnick et al., 1985), volcanic rocks in the Okinawa Trough (Chen et al., 1995), the host rocks for Kuroko at 13 Ma (Farrell and Holland, 1983), and the middle Miocene Kuroko barite (Farrell and Holland, 1983).

data (O'Neil and Taylor, 1969), theoretical calculation by Kieffer (1982) and empirical calibration of natural samples (Savin and Epstein, 1970; Eslinger and Savin, 1973).

Hydrogen isotopic fractionation factors between mica and water are not well defined (Savin and Lee, 1988; Sheppard and Gilg, 1996), but empirical data suggest that the factors are not sensitive to temperature in the range of hydrothermal temperatures (Marumo et al., 1980; Sheppard and Gilg, 1996). Using the factor of −27‰ (Marumo et al., 1980), the δD values of fluids for the Jade micas are calculated to have −3‰ and +1‰.

4.6. Sulfur Isotopic Compositions of Sulfides, Barite, and Native Sulfur

Figure 10 and Table 3 show the S-isotopic compositions of sulfides, sulfates and native sulfur from the active vent area. An aggregate of chalcopyrite and sphalerite (D412-4-1) from the black smoker chimney shows +5.7‰ which falls in the range (+3.2 to +6.1‰) of pyrite and marcasite aggregates (samples RS101, P616-Shoe, P626-5-5-15) from the surface of sediments. These values are significantly lower than the values of H_2S (+7.2 to +8.0‰; Sakai et al., 1990b) dissolved in the vent fluids, indicating isotopic disequilibrium between the two. It may be attributed to a temporal variation in $\delta^{34}S$ of hydrothermal fluids, which has been documented from other active seafloor hydrothermal systems (e.g., Crowe and Valley, 1992).

Fine grained (<1 mm) pyrite and marcasite disseminated in altered sediments and tuffs (P613-2-2-60 to RS118, Table 3) show a large variation from −38.5 to +0.7‰. The variation is attributed to a contribution of biogenic sulfur. The $\delta^{34}S$ values of the Jade barite (P626-3-5-5 and P626-Shoe) range from +21.0 to +22.5‰ and are similar to the present-day seawater sulfate value (+20.8‰; Fig. 10).

A large (>20 cm) specimen (samples RS109-A, B, C) of native sulfur crust on the seafloor shows a wide variation in $\delta^{34}S$ ranging from +6.6 to +11.2‰. The values are mostly higher than those of dissolved H_2S (+7.2 to +8.0‰) in the vent fluids, showing isotopic disequilibrium. This may be explained also by a temporal variation of S dissolved in the fluids. Alternatively, it may be attributed to disequilibrium precipitation of native sulfur. Isotopic disequilibrium is prevalent in many subaerial sulfur deposits (Ueda et al., 1979) because the formation of native sulfur requires the valence change from −2 in fluids. Native sulfur in Jade was formed on the seafloor where fluids were exhaled into cold, oxidizing seawater. It is

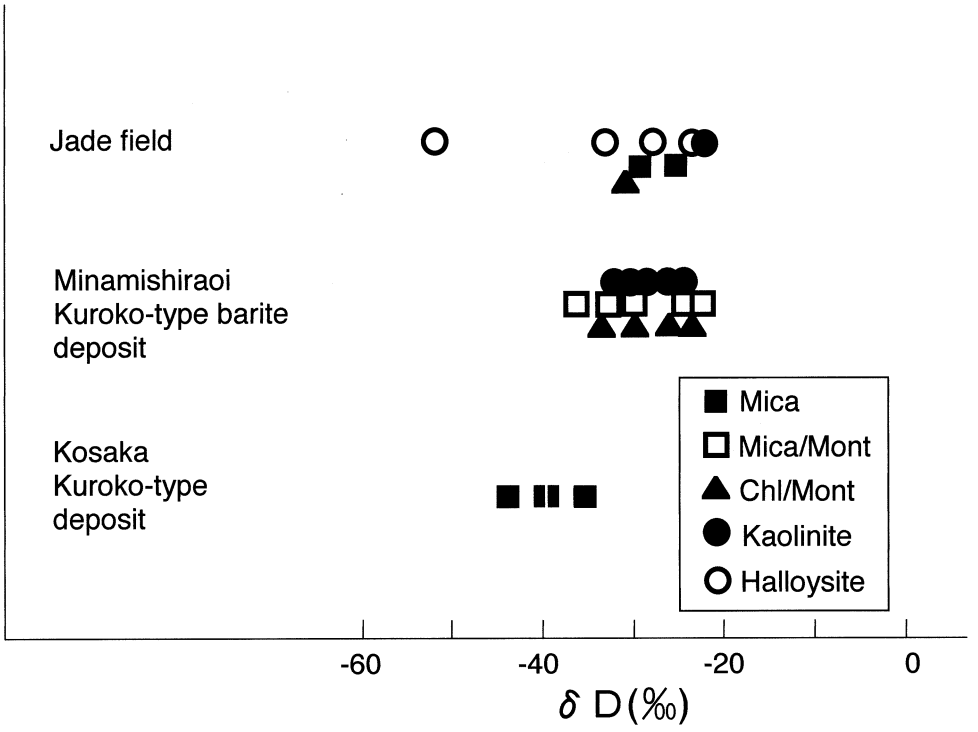

Fig. 7. Hydrogen isotopic compositions of clay minerals from the Jade field, Kosaka (Hattori and Muehlenbachs, 1980) and Minamishiraoi deposits (Marumo, 1989b; Marumo et al., 1995).

likely that sulfur species did not maintain isotopic equilibration under such dynamic conditions where temperatures and fO_2 changed rapidly.

5. DISCUSSION

5.1. Origin of Clay Minerals in the Jade Field

The hydrothermal alteration at Jade is characterized by common occurrences of mica, kaolins (kaolinite and halloysite), Mg-rich chlorite, talc, Chl/Mont and montmorillonite. Among them, mica (Alt et al., 1987; Alt and Jiang, 1991), Chl/Mont (Haymon and Kastner, 1986; Howard and Fisk, 1988), Mg-rich chlorite (Koski et al., 1990), talc (Zierenberg et al., 1993) and montmorillonite-beidellite (Haymon and Kastner, 1986) have been reported in the ridge hydrothermal systems at 21°N East Pacific Rise (EPR), Gorda Ridge, and Guaymas basin. The predominant occurrence of mica at Jade reflects high K^+ (<72 mM/kg) of fluids in comparison with those in the ridge systems, such as those at the 21°N EPR (K^+ = 23.2 to 25.8 mM/kg; Von Damm et al., 1985a) and Guaymas (K^+ = 37.1 to 49.1 mM/kg; Von Damm et al., 1985b).

The occurrences of kaolins (kaolinite and halloysite) also characterize the alteration at Jade. Kaolins are commonly formed by intensive hydrogen metasomatism in subaerially altered rocks (e.g., Nagasawa, 1978). The occurrences of kaolins are not common in other seafloor hydrothermal systems, although the vent fluids at the 21°N EPR and 13°N EPR are acidic (pH = 3.8 at 25°C; Von Damm et al., 1985a and Bower et al., 1988).

The stability of kaolinite, mica, chlorite ($Mg_5Al_2Si_3O_{10}(OH)_8$), and K-feldspar are calculated in terms of the activity ratios of Mg^{2+}/H^+ and K^+/H^+ at temperatures between 50 and 300°C using the data by Johnson et al. (1992). The venting fluids from the black smoker at Jade contain no detectable Mg^{2+} (Sakai et al., 1990a) and the ratios of aK^+/aH^+ are around 3.56 (Fig. 11). The observed aK^+/aH^+ ratios fall near the boundary of the stability fields between mica and K-feldspar, suggesting that the aK^+/aH^+ ratios of the hydrothermal fluids are likely controlled by these minerals. The proposed interpretation is consistent with the data from subaerial geothermal reservoir fluids showing that their K/H ratios are buffered by two minerals (e.g., Hemley, 1959).

The composition of fluids formed by mixing of the vent fluid with seawater plots a linear array (Fig. 11). The alteration mineral formed from the mixed fluids should be K-feldspar at temperatures lower than 250°C and mica and kaolinite would not form from the mixed fluid. This is further demonstrated by the activity ratios of K^+/H^+ and Mg^{2+}/H^+ estimated for the alteration fluids using the isotopic temperatures and mineral assemblages. Fluids were in the stability field of kaolinite at 61°C (P626-Shoe) and 170°C (P613-2-2-60) and in the mica field at 145°C (RS105) and 238°C (RS113). They all plot far left from the mixing line of vent fluids and seawater (Fig. 11). The observed alteration minerals require much lower K^+/H^+ ratios, lower pH, than those predicted from simple mixing. Acidic fluids are consistent with the common occurrence of native sulfur at Jade since it is only stable in low pH.

Acidic condition of the fluids is explained by the oxidation of H_2S either dissolved in the fluids or released from fluids during fluid decompression. If the proposed interpretation is correct,

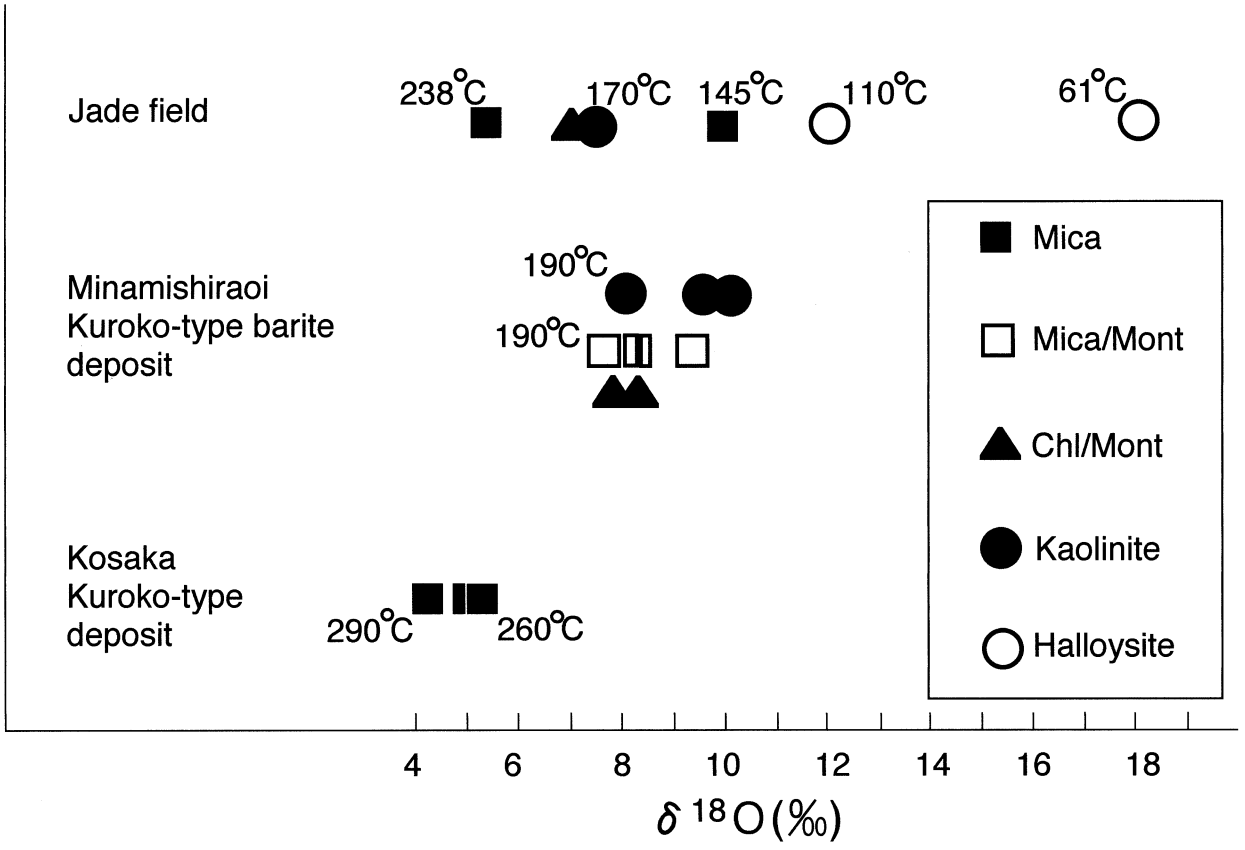

Fig. 8. Oxygen isotopic compositions of clay minerals from Jade compared with the data from Kuroko-type deposits. Isotopic temperatures for Jade samples are calculated using the fractionation factor of Sheppard and Gilg (1996), assuming the seawater value for the fluid. Formation temperatures for the Kosaka and Minamishiraoi clays are recalculated using the isotopic data of clays and filling temperatures of fluid inclusions in quartz and sphalerite associated with the clays. Data sources: Kosaka Kuroko-type deposit (Hattori and Muehlenbachs, 1980), Minamishiraoi Kuroko-type barite deposit (Marumo, 1989b; Marumo et al., 1995).

acidic fluids should be common in many hydrothermal fluids and kaolins should be present in many seafloor hydrothermal systems, but the occurrence of kaolin minerals are only recently reported from Southern EPR (Marumo et al., 1994). It is possible that kaolins may have been overlooked in earlier studies, but there are also several factors favourable for kaolin formation at Jade. The hydrothermal activity at Jade is at relatively shallow water depths, which promotes devolatilization of H_2S from fluids. Gaseous H_2S would be concentrated closer to the seafloor. This is supported by CO_2 venting common in the Jade area (Sakai et al., 1990b). Furthermore, Jade fluids have high S/metals ratios. Upon fluid cooling, H_2S would form metal sulfides, but excess S is available for acidification of fluid in the system with high S/metals ratios.

5.2. Comparison with Middle Miocene Kuroko-Type Deposits

The Jade deposit has been interpreted as a present-day example of Kuroko-type deposits of middle Miocene age in Japan. As described, there are two types of Kuroko-type deposits; polymetallic deposits (represented by the Kosaka deposit) and metal-poor barite deposits (represented by the Minamishiraoi deposit). The two types of deposits show different styles of alteration. The alteration at Kosaka is characterized by mica and Mg-rich chlorite; whereas that at Minamishiraoi is characterized by the dominance of kaolin minerals, a mixed-layer mineral of dioctahedral chlorite and montmorillonite (Chl/Mont), and a mixed-layer mineral of mica and montmorillonite (Mica/Mont). The present-day hydrothermal activity at Jade is not similar to that at metalliferous Kuroko deposits. Instead, it is similar to that at metal-poor barite deposits.

5.2.1. Alteration minerals and formation temperatures

Kaolins occur in several Kuroko-type deposits, but their occurrences are restricted to metal-poor barite deposits formed at temperatures lower than 200°C (Marumo, 1989b; Yoneda, 1993). Isotopic temperatures from Jade are also low: 61 to 170°C for kaolins and 145 to 238°C for mica. Filling temperatures of inclusions in barite in the Jade chimneys range between 150 to 210°C (Halbach et al., 1989b). Venting fluids are also cooler than 220°C except for the black smoker fluids (e.g., Nakamura et al., 1990; Tanaka et al., 1990).

Both the Minamishiraoi deposit and Jade field show kaolins and Chl/Mont as alteration minerals. Isotopic compositions of these clays and their formation temperatures are also very similar (Fig. 9).

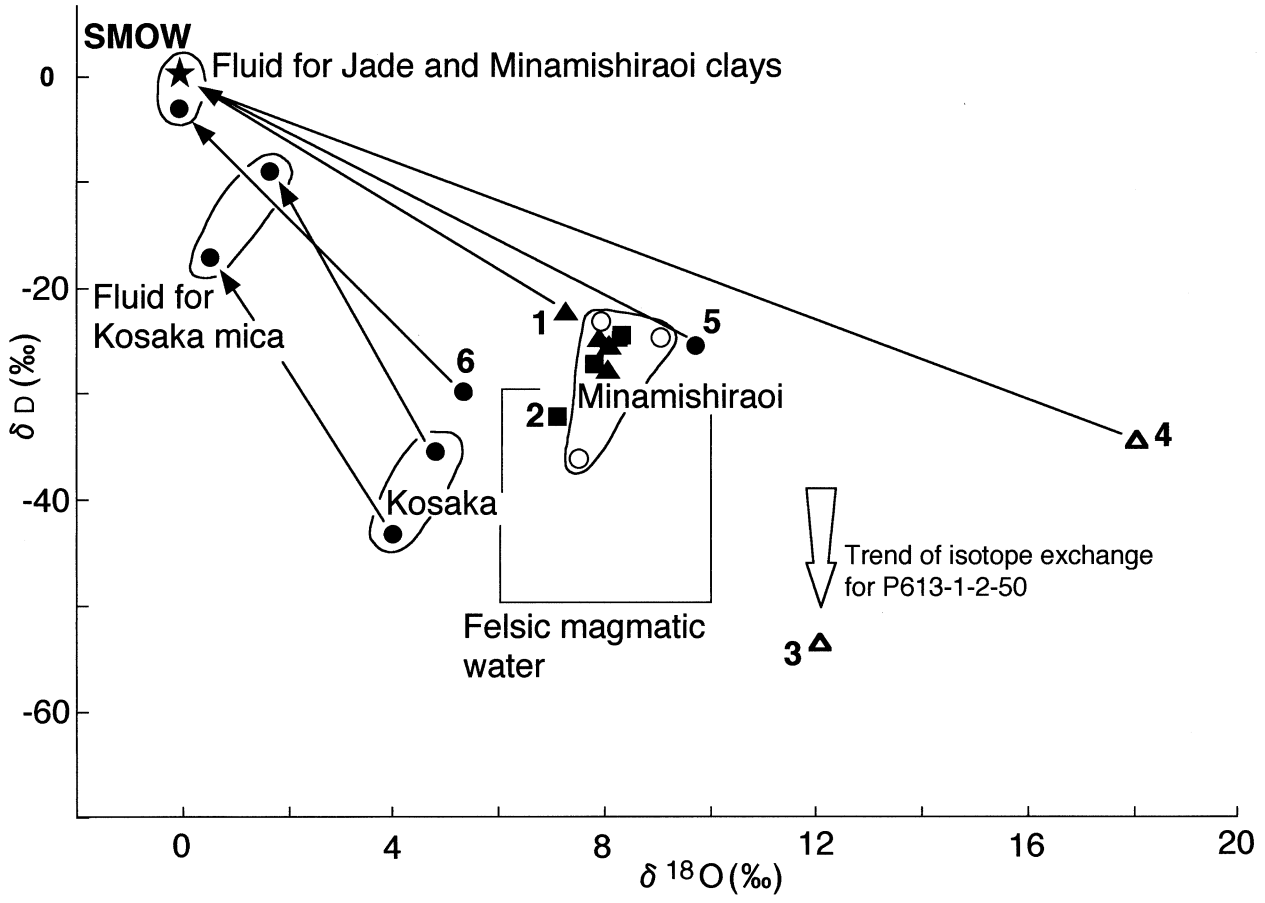

Fig. 9. Hydrogen versus oxygen isotopic compositions for clay minerals and associated fluids. Data sources: Jade field (this study), Kosaka (Hattori and Muehlenbachs, 1980), Minamishiraoi deposits (Marumo, 1989b; Marumo et al., 1995), felsic magmatic water (Taylor, 1992). Solid circles represent mica, open circles denote mixed-layer minerals of mica and montmorillonite (Mica/Mont), solid triangles stand for kaolinite, open triangles for halloysite, solid squares for mixed-layer minerals of dioctahedral chlorite and montmorillonite (Chl/Mont). The solid triangle labeled 1 shows the isotopic compositions for kaolinite (P613-2-2-60) and the fluid at 180°C. The solid square labeled 2 indicates compositions for Chl/Mont (P613-2-2-90). The open triangle labeled 3 shows the compositions of halloysite (P613-1-2-90). The low δD appears to be a result of isotopic exchange. The open triangle labeled 4 shows the compositions for halloysite (P626-Shoe) and the fluids. The solid circle marked 5 is mica (RS105) and the fluid at 145°C. The solid circle labeled 6 is mica (RS113) and the fluid at 238°C. The solid circle directly under the solid star shows the isotopic compositions of the fluid for RS113, at 238°C.

5.2.2. Occurrence of native sulfur

Another similarity between the two is the common occurrence of native sulfur, which is very rare in polymetallic Kuroko-type deposits (Igarashi et al., 1974). The lack of native sulfur in polymetallic Kuroko deposits suggests low S/metals ratios of hydrothermal fluids due to high concentration of heavy metals, whereas hydrothermal fluids for barite-rich Kuroko deposits likely had high S/metals ratios.

The proposed interpretation is supported by the occurrences of native sulfur in other seafloor hydrothermal systems. Native sulfur of the Axial Seamount in the Juan de Fuca Ridge is associated with amorphous silica after the cessation of metal sulfide precipitation (Hannington and Scott, 1988). Native sulfur is also reported in the hydrothermal plumes along the southern EPR from 17°30′S to 18°40′S. These plumes contain halloysite and kaolinite (Marumo et al., 1994) and have high S/Fe molar ratios, higher than 1 (Feely et al., 1994).

5.2.3. Fluid sources

Sulfate minerals from Jade show $^{87}Sr/^{86}Sr$ similar to the present-day seawater value. The isotope data are significantly different from those of the Kosaka deposit. The values for the Kosaka barite (0.7068 to 0.7082; Farrell and Holland, 1983) are much lower than that of the Miocene seawater (0.70849; Koepnick et al., 1985), suggesting a significant contribution of igneous Sr supplied through the reaction with volcanic rocks and/or the direct contribution of magmatic fluids.

The Jade fluids are essentially heated seawater, whereas the fluids for the polymetallic Kosaka deposit are significantly different. Low δD, −22 to −9‰ calculated for the Kosaka fluids suggest a direct contribution of magma fluids (Hattori and Muehlenbachs, 1980). This supports the importance of magmatic fluids for the formation of metal deposits as magmatic fluids can contain high concentrations of base metals (Candela and Holland, 1984; Urabe, 1985, 1987).

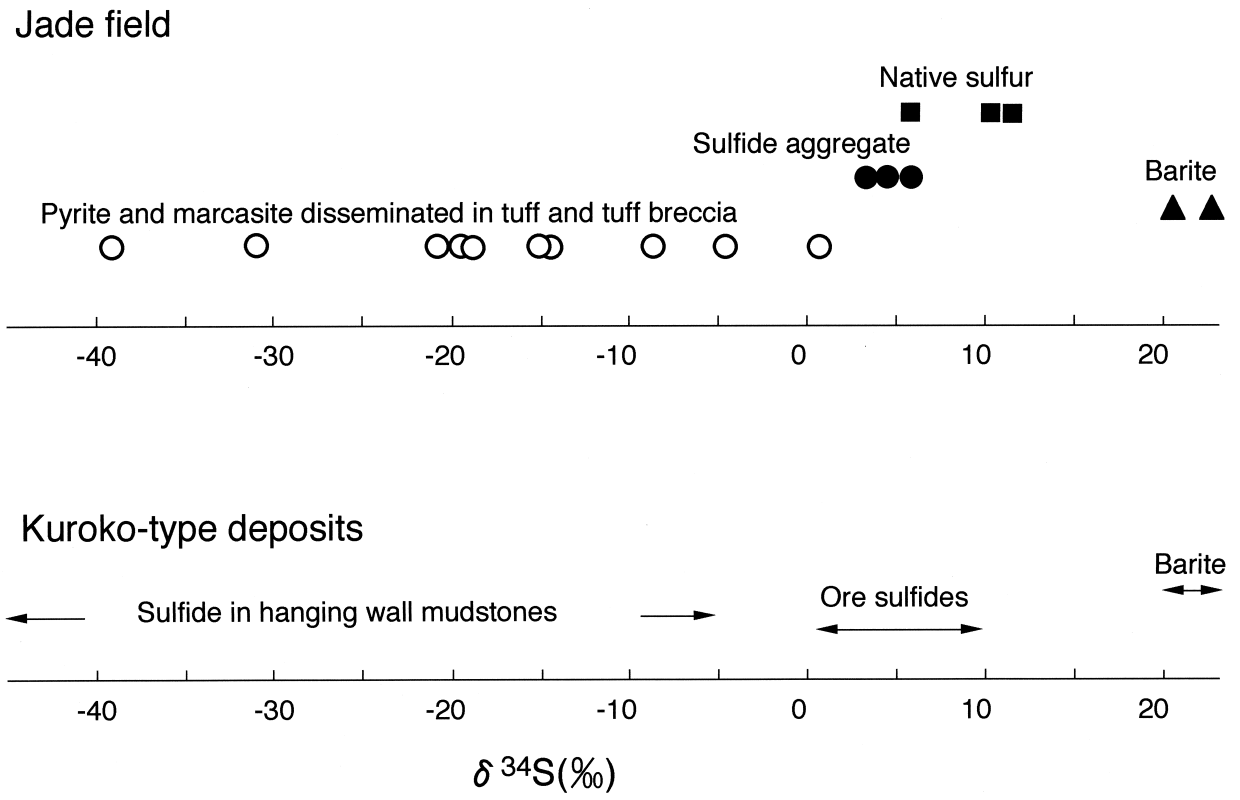

Fig. 10. Sulfur isotopic compositions of sulfides, barite, and native sulfur from the Jade field. Sulfur isotopic data of the middle Miocene Kuroko deposits (Ohmoto et al., 1983) are also shown for comparison.

5.3. Present and Past Hydrothermal Activity at Jade Deposit

The oxygen isotopic data suggest high temperature formation of mica and low temperature formation of kaolin, but the distribution of mica and kaolins (Fig. 1-3) are not well correlated with the present-day heat flow values (Fig. 1-3). For example, kaolin-bearing sites (611, 613, 617, 619) show a wide range in heat flow from 1,043 to over 21,000 mW/m^2, whereas some of mica-bearing sites, such as the site 610, show low heat flow values. The discrepancy between the alteration assemblages and the present heat flow values may be attributed to the change in the hydrothermal flow regime. Fluid flows can be modified with time by sealing of their passages, fluctuation of fluid pressures, and brecciation. The existence of a non-steady flow regime at Jade appears to be supported by a large variation in the $\delta^{34}S$ for the sulfides. Fluid flows are not pervasive enough to homogenize S isotope ratios of the sulfides.

Complicated vertical distributions of kaolins are observed in the 1.5 m depth gravity core at site 613 (Fig. 4-3). The surface tuff (0 to 45 cm depths) contains kaolinite with minor mica, whereas halloysite is predominant in the underlying pumiceous tuffs (80 to 115 cm depths). The O isotopic compositions of the kaolinite (sample P613-2-2-60, $\delta^{18}O = +7.4‰$) and the underlying halloysite (sample P613-1-2-50, $\delta^{18}O = +12.0‰$) suggest the kaolinite near the seafloor formed at higher temperatures (170°C) than the halloysite (110°C). The data appears to reinforce a continuously changing hydrothermal flow regime near the seafloor.

A temporal change in the hydrothermal activity at Jade is further supported by anomalous concentration of heavy metals in sediments due to the fall-out from the past hydrothermal plumes. High concentrations of metals (Fe is up to 1,100 ng/l and Cu is up to 300 ng/l) were observed in the water between 1,300 and 1,100 m water depth, so 100 to 300 m directly above the Jade field, during the R/V Hakurei-maru GH89-3 cruise in 1989 (Shitashima et al., 1990). The values are significantly higher than their background values (less than 200 ng/l Fe, less than 100 ng/l Cu) obtained from the shallower levels. The high metal anomalies must be derived from the Jade field, because there is no other hydrothermal activity in the area.

Many fossil chimneys and mounds, which are not accompanied by fluid discharge, are found in the Jade field (Halbach et al., 1989a, 1993; Nakamura et al., 1990) suggesting more intense polymetallic hydrothermal activity in the past. The temporal change of the hydrothermal activities is evaluated using the metal anomalies in sediments since metalliferous suspended material from hydrothermal plumes may be incorporated in the sediments. The epiclastic sediments from site 611, located about 150 m SE of the black smoker, show metal anomalies from surface to 200 cm depths (Fig. 4-1). The sediments at the site were subject to hydrothermal alteration and the metal anomalies may be due to in-situ hydrothermal activity. Assuming that the anomalies are due to fall-out from the plumes, the anomalies suggest a continuous hydrothermal activity over the past 1,540 yr using the sedimentation rate of 1.3 mm/yr (Tamaki et al., 1989). This rate is in the sedimen-

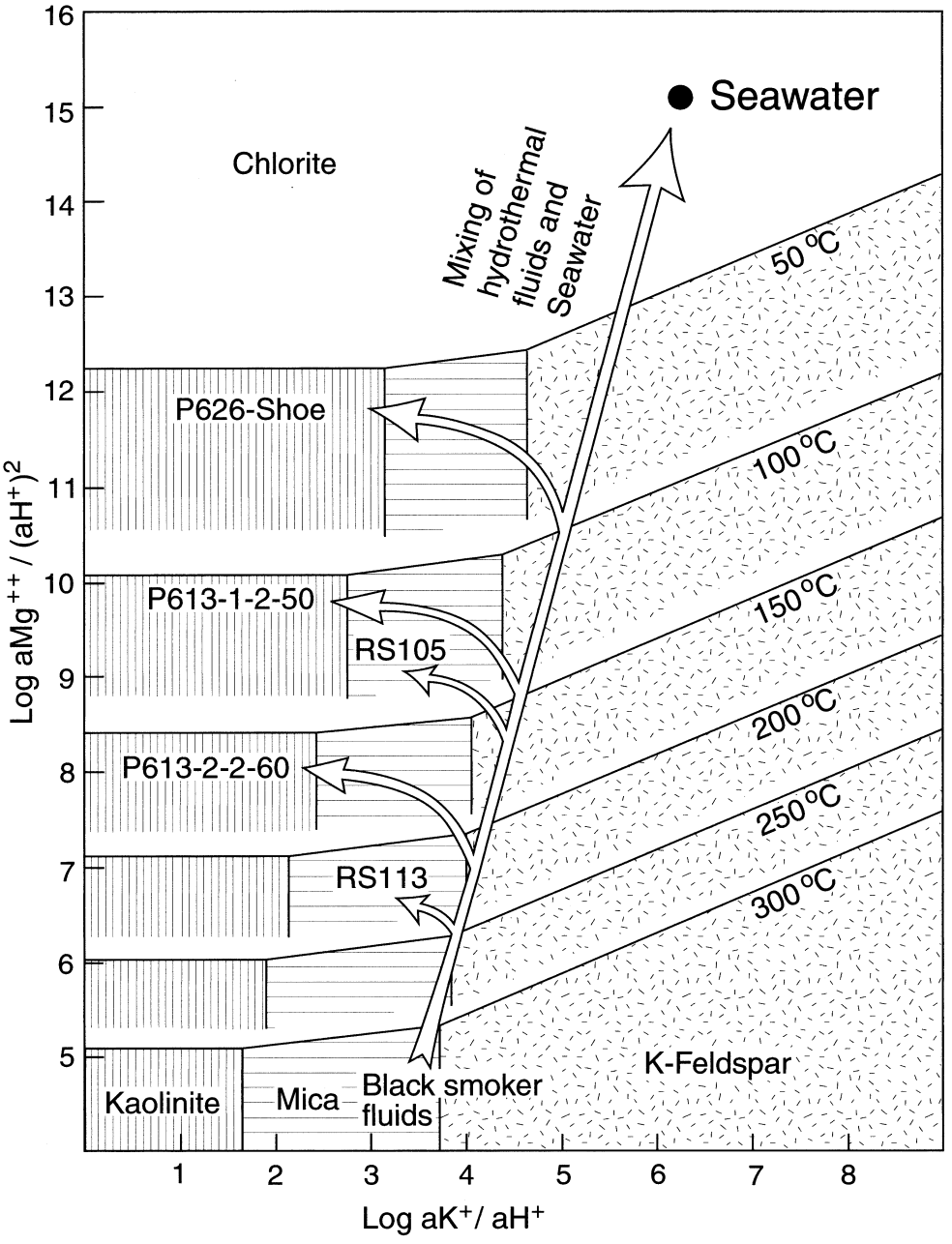

Fig. 11. Stability fields of kaolinite, mica, Mg-Al-chlorite and K-feldspar. They were calculated using the data in Johnson et al. (1991). Logarithmic ratios of aK^+/aH^+ for the fluids from the black smoker are ~3.6 and those of $aMg^{2+}/(aH^+)^2$ are below 5 due to the absence of detectable Mg^{2+}. The compositions for the alteration fluids are plotted using the alteration assemblages and isotopic temperatures. They all plot left of the mixing line. The shift to low pH is explained by sulfuric acid formed by oxidation of H_2S.

tation rates, 1 to 5 mm/yr, in the central Okinawa Trough (Saito and Ikehara, 1992).

The site 608 in the bottom of the Izena Cauldron (Fig. 1-3) records low heat flow (270 mW/m^2; Fig. 1-3; Kinoshita, 1990) and the sediments contains abundant calcareous nannoplanktons with no evidence of hydrothermal alteration. Unfortunately, the core was not suitable for this study because of a disturbance due to subsolifluction (Nakamura et al., 1990).

The epiclastic sediments from the site 626 (Fig. 4-2), ~200 m E of the black smoker, were not subject to apparent alteration, but they show anomalous high concentrations of Cu, Zn, As, Ag, and Pb at 100 to 300 cm depths and of Ba at 100 to 150 cm depths. Assuming rapid accumulation of tuffs at the depth between 40 and 100 cm, the metal anomalies correspond to 300 to 1,800 ybp for base metals and 300 to 700 ybp for Ba precipitation.

The sediments at the site 609, 2.5 km from the Jade field, show high concentrations of Cu, Zn, Ag, and Pb from the depth

of 40 to 100 cm (corresponding to 300 to 770 ybp) and anomalous concentrations of As and Ba at depths from 0 to 100 cm (corresponding from the present to 770 ybp) (Fig. 2-2). The highest values of Zn and Hg occur at the depth of 75 cm. To confirm the proposed interpretation, we tried to find Fe-oxyhydroxide in the sediments because Fe is always the major component of suspended material in hydrothermal plumes (Cowen et al., 1986; Feely et al., 1990; Marumo et al., 1994). If the Cu, Zn, and Pb in the sediments were originated from hydrothermal plumes, they should be associated with Fe-oxyhydroxides. Although TEM examination failed to identify discrete grains of Fe-oxyhydroxides, montmorillonite grains down to the depth of 100 cm are found to be coated with Fe (Fig. 3-2). Fe-oxyhydroxide was absorbed on the surface of montmorillonite grains. Detrital montmorillonite grains slowly settling down to the seafloor became coated with Fe when they pass through the plume head in the water column.

The metal anomalies at the site 609 are clearly due to hydrothermal activities at Jade because no other hydrothermal activities have been reported in the area. A site 33 km N of the Izena Cauldron contains an Fe-oxide mound with high concentrations of Zn (<220 ppm), As (<240 ppm), Mo (<2,500 ppm), Sb (<52 ppm) (Kimura et al., 1988). Another hydrothermal area, called Iheya deep (Mn <26.3 wt%, Zn <0.51 wt%, As <5,100 ppm, Ag <290 ppm, Sb <1,400 ppm, Hg <310 ppm), occurs 34 km NW from the Izena Cauldron (Kimura et al., 1989).

The site 628 is ~8 km away from the Jade field, but there are no metal anomalies in the sediments. It may be too far from the venting sites. Alternatively, the shallow water depth of the site 628 (less than 1,000 m water depth) may have prevented sediments from receiving the fall-out. Hydrothermal plumes rise and remain at a certain depth and spread laterally up to several kms. The Fe- and Cu-rich water layer at 1,100 to 1,300 m water depths is apparently stagnant around the Izena Cauldron, suggesting rises of 100 to 300 m from the venting sites. The height of the plumes is comparable with those in other seafloor hydrothermal systems, cf: buoyant height 50 to 200 m at the EPR 8°40′ to 11°50′N (Baker et al., 1994), and the EPR 13°33′ to 18°40′S (Feely et al., 1996). In the Jade area, plumes may spread to W, but not to NE because of shallow water depths (Fig. 1-2). Metal anomalies may be found in the sediments to SW, such as the site 609, but not to E, such as the site 628.

The Cu, Zn, As, Ag, and Pb anomalies are observed at 40 to 240 cm depths and that Ba anomaly is observed at 40 to 90 cm depths at the site 626, whereas the Cu, Zn, Ag, and Pb anomalies occur at 40 to 100 cm depths and that As and Ba anomalies are from 0 to 100 cm depths at the site 609. The different depth profiles of anomalies are to be expected because greater amounts of Cu, Zn, As, Ag, and Pb are expected closer to the vent sites. Moreover, sulfides fell from hydrothermal plumes first (Feely et al., 1996). This implies that more sulfides should be found at the site 626, 200 m away from the venting site, than at the site 609, 2.5 km away from the venting site.

The wt. ratios of (Cu+Zn+Pb)/Ba are higher at greater depths of cores: 348 at a 194 cm depth (Cu = 8, 100 ppm, Zn = 1.25 wt%, Ba = 120 ppm, and Pb = 2.1 wt%) and 0.35 at a depth of 134 cm. The evidence further confirms that past hydrothermal fluids were metal-rich. The ratios for the sample P609-4-5-35 (Table 1) is 4.2, using the background values obtained from P628-4-4-10 (Table 1). The value of 4.2 is larger than that of the Minamishiraoi deposit (less than 0.1), but lower than that of the Kosaka deposit (over 10).

6. CONCLUSIONS

1. Seafloor hydrothermal activity at Jade has resulted in the dissolution of calcareous nannoplanktons and the formation of native sulfur, sulfides, barite, dolomite, mica, kaolins (kaolinite and halloysite), Mg-rich chlorite, talc, montmorillonite, and Chl/Mont in sediments and tuffs.
   The variation in the alteration mineral assemblages is primarily explained by the mixing of hot hydrothermal fluids with cold seawater. Mica form at temperatures greater 145°C, whereas kaolins form at temperatures lower than 170°C from fluids with greater fractions of cold seawater. Abundant kaolins suggest acidification of fluids by oxidation of H_2S close to the seafloor. High ratios of S/metals in the present-day fluids at Jade contributed to the formation of sulfuric acid. It is consistent with the abundant occurrences of native sulfur, which was formed from excess H_2S in the fluids, which does not form metal sulfides.
2. Fall-out of hydrothermal plumes caused high metal concentrations of unaltered sediments distant from the vent areas. Detrial montmorillonite grains were coated with Fe oxyhydroxides during their suspension in seawater and incorporated into the sediments.
3. The H and Sr isotopic compositions of clay and sulfate minerals suggest hydrothermal fluids of essentially seawater origin. The isotopic formation temperatures for mica are higher than kaolinite and that for kaolinite higher than those for halloysite.
4. The $\delta^{34}S$ for barite and anhydrite are very similar to the present-day seawater sulfate. Native sulfur shows a large variation in $\delta^{34}S$, due to its disequilibrium precipitation from fluids during the exhalation of hot fluids into cold oxidizing seawater. Sulfides in the sediments far from the vent areas were formed by bacterial reduction of marine sulfate, as shown by a large variation in $\delta^{34}S$.
5. The hydrothermal activity at Jade is very similar to those for low temperature metal-poor, Kuroko-type barite deposits of middle Miocene age. Hydrothermal activity ~1,800 to 300 ybp was more metalliferous, producing hydrothermal plumes and sulfide chimneys and mounds with higher concentrations of heavy metals. The past activity at Jade was probably similar to that for polymetallic Kuroko-type deposits of middle Miocene age.

Acknowledgments—Samples used in this study were obtained during the Geological Survey of Japan GH-89-3 cruise to Okinawa Trough (Y. Okuda, chief scientist) with research vessel Hakurei-maru. We thank shipboard scientists and crew members for their technical support. We are particularly indebted to T. Urabe and K. Nakamura (Geological Survey of Japan) for their advises during this project. We also thank R. A. Feely and H. Kodama for their helpful comments. Funding for this research was provided by Research grants from the Geological Survey of Japan (K.M) and the Natural Sciences and Engineering Research Council of Canada (KHH).

REFERENCES

Alt J. C. and Jiang W.-T. (1991) Hydrothermally precipitated mixed-layer illite-smectite in recent massive sulfide deposits from the sea floor. *Geology* **19,** 570–573.

Alt J. C., Lonsdale P., Haymon R., and Muehlenbachs K. (1987) Hydrothermal sulfide and oxide deposits on seamounts near 21°N, East Pacific Rise. *Geological Society of America Bulletin* **98,** 157–168.

Baker E. T., Feely R. A., Mottle M. J., Sansone F. J., Wheat C. G., Resing J. A., and Lupton J. E. (1994) Hydrothermal plumes along the East Pacific Rise, 8°40′–11°50′N: Plume distribution and relationship to the apparent magmatic budget. *Earth Planet. Sci. Lett.* **128,** 1–17.

Bower T. S., Campbell A. C., Measures C. I., Spivack A. J., Khadem M., and Edmond J. M. (1988) Chemical controls on the composition of vent fluids at 13°–11°N and 21°N, East Pacific Rise. *J. Geophys. Res.* **93,** 4522–4536.

Candela, P. A. and Holland H. D. (1984) The partitioning of copper and molybdenum between silicate melts and fluids. *Geochim. Cosmochim. Acta* **48,** 373–380.

Chen C. H., Lee T., Shieh Y. N., Chen C. H. and Hsu W. Y. (1995) Magmatism at the onset of back-arc basin spreading in the Okinawa Trough. *J. Volcan. Geotherm. Res.* **69,** 313–322.

Chiba H., Sakai H., Ishibashi J., and Urabe T. (1992) Sr isotopic study of seafloor hydrothermal system in mid-Okinawa trough. (abstr.) *29th International Geological Congress.* **3–3,** pp. 754.

Clayton R. N. and Mayeda T. K. (1963) The use of bromine pentafluoride in the extraction of oxygen from oxides and silicates for isotopic analysis. *Geochim. Cosmochim. Acta* **27,** 43–45.

Cowen J. P., Massoth G. J., and Baker E. T. (1986) Bacterial scavenging of Mn and Fe in a mid-to far-field hydrothermal particle plume. *Nature* **322,** 169–171.

Crowe, D. E. and Valley, J. W. (1992) Laser microprobe study of sulfur isotope variation in a sea-floor hydrothermal spire, Axial Seamount, Juan de Fuca Ridge, eastern Pacific. *Chem. Geol.* **101,** 63–70.

Eldridge C. S., Barton P. B. Jr., and Ohmoto H. (1983) Mineral textures and their bearing on formation of the Kuroko orebodies. In *The Kuroko and Related Volcanogenic Massive Sulfide Deposits* (ed. H. Ohmoto and B. J. Skinner) *Econ. Geol. Mon.* **5,** 241–281.

Eslinger E. V. and Savin S. M. (1973) Mineralogy and oxygen isotope geochemistry of the hydrothermally altered rocks of the Ohaki-Broadlands, New Zealand geothermal area. *Amer. J. Sci.* **273,** 240–267.

Farrell C. W. and Holland H. D. (1983) Strontium isotope geochemistry of the Kuroko deposits. In *The Kuroko and Related Volcanogenic Massive Sulfide Deposits* (ed. H. Ohmoto and B. J. Skinner); *Econ. Geol. Mon.* **5,** 302–319.

Feely R. A., Baker E. T., Marumo K., Urabe T., Ishibashi J., Gendron J., Lebon G. T., and Okamura K. (1996) Hydrothermal plume particles and dissolved phosphate over the superfast-spreading southern East Pacific Rise. *Geochim. Cosmochim. Acta* **60,** 2297–2323.

Feely R. A., Marumo K., Urabe T., Baker E. T., Gendron J. F., and Lebon G. T. (1994) Element chemistry of hydrothermal particles along the superfast-spreading Southern East Pacific Rise, 13°50′–18°40′S. (abstr.) *EOS* **75–44,** 321.

Feely R. A., Geiselman E. T., Baker E. T., and Massoth G. J. (1990) Distribution and composition of hydrothermal plume particles from the ASHES vent field at Axial volcano, Juan de Fuca Ridge. *J. Geophys. Res.* **95,** 12855–12873.

Franklin J. M., Lydon J. W., and Sangster D. F. (1981) Volcanic-associated massive sulfide deposits. *Econ. Geol. 75th Anniversary Volumes*, 485–627.

Halbach P., Nakamura K., and others (1989a) Probable modern analogue of Kuroko-type massive sulphide deposits in the Okinawa Trough back-arc basin. *Nature* **338,** 496–499.

Halbach P., Pracejus B., and Marten A. (1993) Geology and mineralogy of massive sulfide ores from the central Okinawa Trough, Japan. *Econ. Geol.* **88,** 2210–2225.

Halbach P., Wahsner M., Kaselitz L., Sakai H., and Hein U. (1989b) The Jade hydrothermal field in the Okinawa trough—first discovery of massive sulfides in an intercontinental back-arc basin. *Proceedings of the 6th International Symposium on Water-Rock-Interaction*, 279–283.

Hannington M. D. and Scott S. D. (1988) Mineralogy and geochemistry of a hydrothermal silica-sulfide-sulfate spire in the caldera of Axial Seamount, Juan de Fuca Ridge. *Canadian Mineral.* **26,** 603–626.

Hattori K. and Muehlenbachs K. (1980) Marine hydrothermal alteration at a Kuroko ore deposits, Kosaka, Japan. *Contrib. Mineral. Petrol.* **74,** 285–292.

Haymon R. M. and Kastner M. (1986) The formation of high temperature clay minerals from basalt alteration during hydrothermal discharge on the East Pacific Rise axis at 21°N. *Geochim. Cosmochim. Acta* **50,** 1933–1939.

Haymon R. M. and Kastner M. (1981) Hot spring deposits on the East Pacific Rise at 21°N. *Earth Planet. Sci. Lett.* **53,** 363–381.

Hemley, J. J. (1959) Some mineralogical equilibria in the system K_2O-Al_2O_3-SiO_2-H_2O. *Amer. Jour. Science* **257,** 241–270.

Howard K. J. and Fisk M. R. (1988) Hydrothermal alumina-rich clays and boehmite on the Gorda Ridge. *Geochim. Cosmochim. Acta* **52,** 2269–2279.

Igarashi T., Okabe K., and Yajima J. (1974) Massive barite deposits in west Hokkaido. In *Geology of Kuroko Deposits* (ed. S. Ishihara); *Soc. Mining Geol. Japan, Spec. Issue* **6,** 39–44.

Ishibashi J., Gamo T., Sakai H., Nojiri Y., Igarashi G., Shitashima K., and Tsubota H. (1988) Geochemical evidence for hydrothermal activity in the Okinawa Trough. *Geochem. J.* **22,** 107–114.

Johnson J., Oelkers E. H., and Helgeson H. C. (1991) SUPCRT92: A software package for calculating the standard molal thermodynamic properties of minerals, gases, aqueous species, and reactions from 1 to 500 bars and 0° to 200°C. Laboratory of Theoretical Geochemistry, University of California, Berkeley.

Kieffer S. W. (1982) Thermodynamics and lattice vibrations of minerals: 5. Applications to phase equilibria, isotopic fractionation, and high pressure thermodynamic properties. *Rev. Geophys. Space Phys.* **20,** 827–849.

Kimura M., Tanaka T., Kyo M., Ando M., Oomori T., Izawa E. and Yoshikawa I. (1989) Study of topography, hydrothermal deposits and animal colonies in the middle Okinawa Trough hydrothermal areas using the submersible "SHINKAI 2000" system. *The 5th Symposium on Deep-sea Research Using the Submersible "SHINKAI 2000" System*, 224–244 (in Japanese).

Kimura M., Uyeda S., Kato Y., Tanaka T., Yamano M., Gamo T., Sakai H., Kato S., Izawa E. and Oomori T. (1988) Active hydrothermal mounds in the Okinawa Trough backarc basin, Japan. *Tectonopysics* **145,** 319–324.

Kinoshita M. (1990) Heat flow measurements at the Izena Cauldron in the Okinawa Trough. *GH-89 Cruise Report, Geological Survey of Japan* 130–149 (in Japanese).

Koepnick R. B., Burke W. H., Denison R. E., Hetherington E. A., Nelson H. F., Otto J. B., and Waite L. E. (1985) Construction of the seawater $^{87}Sr/^{86}Sr$ curve for the Cenozoic and Cretaceous: Supporting data. *Chem. Geol.* **58,** 55–81.

Koski R. A., Zierenberg R. A., Shanks III W. C., and Campbell A. C. (1990) Chemical and isotopic characteristics of sulfide deposits, hydrothermal fluids, and sediment alteration at Escanaba Trough, Southern Gorda Ridge. (abstr.) *EOS* **71,** 1565.

Kulla J. B. (1979) Oxygen and hydrogen isotope fractionation factors determined in experimental clay-water systems. Unpubl. Ph. D. thesis, University of Illinois at Urbana-Champaign, USA.

Kulla J. B. and Anderson T. F. (1978) Experimental oxygen isotope fractionation between kaolinite and water. *Short Papers 4th Intl. Conf. Geochron. Cosmochrn. Isotope Geol., U. S. Geol. Surv. Open-File Rept. 78-701,* 234–235.

Lawrence J. R. and Taylor H. P. Jr. (1972) Hydrogen and oxygen isotopic systematics in weathering profiles. *Geochim. Cosmochim. Acta* **36,** 1377–1393.

Lawrence J. R. and Taylor H. P. Jr. (1971) Deuterium and oxygen-18 correlation: Clay minerals and hydroxides in Quaternary soils compared to meteoric waters. *Geochim. Cosmochim. Acta* **35,** 993–1003.

Lee C. S., Shor Jr. G. G., Bibee L. D., Lu R. S., and Hilde T. W. C. (1980) Okinawa Trough: origin of a back-arc basin. *Mar. Geol.* **35,** 219–241.

Letouzey J. and Kimura M. (1986) The Okinawa Trough: Genesis of a

back-arc basin developing along a continental margin. *Tectonophys.* **125,** 209–230.

Lorimer G. W. (1987) Quantitative X-ray microanalysis of thin specimens in the transmission electron microscope; a review. *Mineral. Mag.* **51,** 49–60.

Marumo K. (1989a) The barite ore fields of Kuroko-type of Japan. In *Nonmetalliferous Stratabound Ore Fields* (ed. M. K. De Brodtkorb), Chap. 10, pp. 201–231. Van Nostrand Reinhold.

Marumo K. (1989b) Genesis of kaolin minerals and pyrophyllite in Kuroko deposits of Japan: Implications for the origins of the hydrothermal fluids from mineralogical and stable isotope data. *Geochim. Cosmochim. Acta* **53,** 2915–2924.

Marumo K., Feely R. A., and Urabe T. (1994) Fe-oxyhydroxide and clay minerals suspended in the neutrally buoyant plumes, EPR 14–19°S fast spreading center. (abstr.) *EOS* **75–44,** 321.

Marumo K., Longstaffe F. J., and Matsubaya O. (1995) Stable isotope geochemistry of clay minerals from fossil and active hydrothermal systems, southwestern Hokkaido, Japan. *Geochim. Cosmochim. Acta* **59,** 2545–2559.

Marumo K., Nagasawa K., and Kuroda Y. (1980) Mineralogy and hydrogen isotope geochemistry of clay minerals in the Ohnuma geothermal area, northeastern Japan. *Earth Planet. Sci. Lett.* **47,** 255–262.

McMurtry G. M., Wang C.-H., and Yeh H.-W. (1983) Chemical and isotopic investigations into the origin of clay minerals from the Galapagos hydrothermal mounds field. *Geochim. Cosmochim. Acta* **47,** 475–489.

McMurtry G. M. and Yeh H.-W. (1981) Hydrothermal clay mineral formation of East Pacific Rise and Bauer Basin sediments. *Chem. Geol.* **32,** 189–205.

Nagasawa K. (1978) Kaolin minerals. In *Clays and clay minerals of Japan* (ed. T. Sudo and S. Shimoda), Chap. 5, pp. 189–219. Elsevier.

Nagumo S., Kinoshita H., Kasahara J., Ouchi T., Tokuyama H., Asanuma T., Koresawa S., and Akiyoshi H. (1986) Report on DELP 1984 Cruises in the Middle Okinawa Trough-2: Seismic structural studies. *Bull. Earthq. Res. Inst. Univ. Tokyo* **61,** 167–202.

Nakamura K., Marumo K., and Aoki M. (1990) Discovery of a black smoker vent and a pockmark emitting CO_2-rich fluid on the seafloor hydrothermal mineralization field at the Izena Cauldron in the Okinawa Trough. *6th Symposium on Deep-sea Research using the Submersible "SHINKAI 2000" System* 33–50 (in Japanese with English abstract).

Ohmoto H., Mizukami M., Drummond S. E., Eldridge C. S., Pisutha-Arnond V., and Lenagh T. C. (1983) Chemical processes of Kuroko formation. In *The Kuroko and Related Volcanogenic Massive Sulfide Deposits* (ed. H. Ohmoto and B. J. Skinner); *Econ. Geol. Mon.* **5,** 570–604.

O'Neil J. R. and Taylor H. P. Jr. (1969) The oxygen isotope equilibrium between muscovite and water. *J. Geophys. Res.* **74,** 6012–6022.

Saito H. and Ikehara K. (1992) Sediment discharge of Japanese rivers, and sedimentation rate and carbon content of marine sediments around the Japanese Islands. *Chishitsu News* **452,** 59–64 (in Japanese).

Sakai H., Gamo T., Kim E-S., Shitashima K., Yanagisawa F., Tsutsumi M., Ishibashi J., Sano Y., Wakita H., Tanaka T., Matsumoto T., Naganuma T., and Mitsuzawa K. (1990a) Unique chemistry of the hydrothermal solution in the mid-Okinawa Trough Backarc Basin. *Geophys. Res. Lett.* **17,** 2137–2140.

Sakai H., Gamo T., Kim E.-S., Tsutsumi M., Tanaka T., Ishibashi J., Wakita H., Yamano M., and Oomori T. (1990b) Venting of carbon dioxide-rich fluid and hydrate formation in Mid-Okinawa Trough backarc basin. *Science* **248,** 1093–1096.

Savin M. S. and Lee M. (1988) Isotope studies of phyllosilicates. In *Hydrous Phyllosilicates* (ed. S. W. Bailey); *Review in Mineralogy, Mineralogical Society of America* **19,** 189–223.

Savin M. S. and Epstein S. (1970) The oxygen and hydrogen isotope geochemistry of clay minerals. *Geochim. Cosmochim. Acta* **34,** 25–42.

Sheppard S. M. F. and Gilg H. A. (1996) Stable isotope geochemistry of clay minerals. *Clay Minerals* **31,** 1–21.

Shitashima K., Kumamoto Y., and Ishibashi J. (1990) Geochemical study of the hydrothermal activity in the Okinawa Trough. *GH89–3 cruise report 191–197*. Geological Survey of Japan (in Japanese).

Sverjensky D. A. and Sahai N. (1996) Theoretical prediction of single-site surface-protonation equilibrium constants for oxides and silicates in water. *Geochim. Cosmochim. Acta* **60,** 3773–3797.

Tamaki Y., Oomori T., and Taira H. (1989) Chemical compositions and sedimentation rates of epiclastic sediments around the seafloor hydrothermal systems in the Okinawa Trough (abstr.) *Geochem. Soc. Japan 1989 meeting*. 180 (in Japanese).

Tanaka T., Hotta H., Sakai H., Ishibashi J., Oomori T., Izawa E., and Oda N. (1990) Occurrence and distribution of the hydrothermal deposits in the Izena Hole. Central Okinawa Trough. *The 6th symposium on Deep-sea Research using the Submersible "SHINKAI 2000" System*, 11–26 (in Japanese with English abstract).

Tanaka Y. (1990) Calcareous nannoplanktons at the Izena Cauldron in the Okinawa Trough. *GH-89 Cruise Report, Geological Survey of Japan*, 160–162 (in Japanese with English abstract).

Tanimura S., Date J., Takahashi T., and Ohmoto H. (1983) Geological setting of the Kuroko deposits, Japan. Part 2. Stratigraphy and structure of the Hokuroku district. In *The Kuroko and Related Volcanogenic Massive Sulfide Deposits* (ed. H. Ohmoto and B. J. Skinner); *Econ. Geol. Mon.* **5,** 24–38.

Taylor B. E. (1992) Degassing of H_2O from rhyolite magma during eruption and shallow intrusion, and the isotopic composition of magmatic water in hydrothermal systems. *Rept. Geol. Surv. Japan.* **279,** 190–194.

Tessier A., Campbell P. G. C., and Bisson M. (1979) Sequential extraction procedure for the speciation of particulate trace metals. *Analytical Chemistry* **51,** 844–851.

Ueda A., Sakai H., and Susaki, A. (1979) Isotopic compositions of volcanic native sulfur from Japan. *Geochem. J.* **13,** 269–275.

Urabe T. (1985) Aluminous granite as a source magma of hydrothermal ore deposits: An experimental study. *Econ. Geol.* **80,** 148–157.

Urabe T. (1987) The effect of pressure on the partition ratios of lead and zinc between vapor and rhyolite melts. *Econ. Geol.* **82,** 1049–1052.

Von Damm K. L., Edmond J. M., Grant B., Measures C. I., Walden B., and Weiss R. F. (1985a) Chemistry of submarine hydrothermal solutions at 21°N, East Pacific Rise. *Geochim. Cosmochim. Acta* **49,** 2197–2220.

Von Damm K. L., Edmond J. M., Measures C. I., and Grant B. (1985b) Chemistry of submarine hydrothermal solutions at Guaymas Basin, Gulf of California. *Geochim. Cosmochim. Acta* **49,** 2221–2237.

Yamano M., Uyeda S., Foucher J. P., and Sibuet J. C. (1989) Heat flow anomaly in the middle Okinawa Trough. *Tectonophys.* **159,** 307–318.

Yoneda T. (1993) Barite ores and alteration minerals of the Minamishiraoi Kuroko-type barite deposit, southwestern Hokkaido, Japan: Implication for the environment of ore formation. *Resource Geology Special Issue, No. 17 "Proceeding of the 29th International Geological Congress 1992,"* 120–131.

Zierenberg R., Koski R. A., Morton J. L., Bouse R. M., and Shanks III W. C. (1993) Genesis of massive sulfide deposits on a sediment-covered spreading center, Escanaba Trough, Southern Gorda Ridge. *Econ. Geol.* **88,** 2069–2098.